Stem Cell Reports
Article
OPEN ACCESS

Ex Vivo Expansion and In Vivo Self-Renewal of Human Muscle Stem Cells

Gregory W. Charville,[1,2] Tom H. Cheung,[1,3] Bryan Yoo,[1] Pauline J. Santos,[1] Gordon K. Lee,[4] Joseph B. Shrager,[5] and Thomas A. Rando[1,6,*]

[1]Paul F. Glenn Laboratories for the Biology of Aging and Department of Neurology and Neurological Sciences, Stanford University School of Medicine, Stanford, CA 94305, USA
[2]Department of Developmental Biology, Stanford University School of Medicine, Stanford, CA 94305, USA
[3]Division of Life Science, The Hong Kong University of Science and Technology, Clear Water Bay, Hong Kong 999077, China
[4]Division of Plastic Surgery, Department of Surgery, Stanford University School of Medicine, Stanford, CA 94305, USA
[5]Division of Thoracic Surgery, Department of Cardiothoracic Surgery, Stanford University School of Medicine and VA Palo Alto Health Care System, Stanford, CA 94305, USA
[6]Neurology Service and Rehabilitation Research and Development Center of Excellence, Veterans Affairs Palo Alto Health Care System, Palo Alto, CA 94304, USA
*Correspondence: rando@stanford.edu
http://dx.doi.org/10.1016/j.stemcr.2015.08.004

SUMMARY

Adult skeletal muscle stem cells, or satellite cells (SCs), regenerate functional muscle following transplantation into injured or diseased tissue. To gain insight into human SC (huSC) biology, we analyzed transcriptome dynamics by RNA sequencing of prospectively isolated quiescent and activated huSCs. This analysis indicated that huSCs differentiate and lose proliferative potential when maintained in high-mitogen conditions ex vivo. Further analysis of gene expression revealed that p38 MAPK acts in a transcriptional network underlying huSC self-renewal. Activation of p38 signaling correlated with huSC differentiation, while inhibition of p38 reversibly prevented differentiation, enabling expansion of huSCs. When transplanted, expanded huSCs differentiated to generate chimeric muscle and engrafted as SCs in the sublaminar niche with a greater frequency than freshly isolated cells or cells cultured without p38 inhibition. These studies indicate characteristics of the huSC transcriptome that promote expansion ex vivo to allow enhanced functional engraftment of a defined population of self-renewing huSCs.

INTRODUCTION

In adult mammals, skeletal muscle is regenerated by a population of tissue-resident muscle stem cells, also known as satellite cells (SCs). Quiescent SCs in uninjured muscle are activated in response to injury or disease (Mauro, 1961). Upon activation, SCs undergo a proliferative expansion, yielding a pool of muscle progenitor cells that subsequently fuse to form functional multinucleate muscle fibers (Snow, 1978). In mice, transplanted SCs are capable of engrafting as constituents of multinucleate muscle fibers or as self-renewed muscle stem cells (Collins et al., 2005). When transplanted into dystrophin-deficient mdx mice, wild-type SC-derived muscle progenitors fuse to regenerating host fibers and restore dystrophin expression (Karpati et al., 1989; Partridge et al., 1989). Transplantation of allogeneic muscle progenitors or of genetically corrected autologous muscle progenitors is, therefore, a promising approach to treating inherited muscle diseases, such as Duchenne muscular dystrophy. However, owing to a limited understanding of human SC (huSC) biology, it is still unclear as to what extent findings from mouse studies will translate to human cell-based therapies.

A major barrier to the development of stem cell-based therapies is the inability to generate large numbers of transplantable stem cells with the potential to both self-renew and differentiate. In general, the contribution of donor SCs to muscle regeneration has been shown to correlate with the number of cells transplanted (Bosnakovski et al., 2008; Sacco et al., 2008). Although transplantation of SCs in association with donor muscle fibers has been shown to enhance engraftment efficiency (Collins et al., 2005; Hall et al., 2010), biopsies, surgical specimens, and post-mortem tissue donations are expected to yield few cells relative to the number that will be required for therapeutic huSC engraftment, and techniques for the growth and manipulation of progenitor cells ex vivo are, therefore, expected to be an important element of cell-based therapies. Culturing huSCs also will be important for therapies involving gene correction of autologous cells, which will need to be engineered, selected, and expanded ex vivo. These technical challenges are compounded by the loss of regenerative potential that occurs when SCs are grown in culture. In studies of mouse SCs, expansion in culture for as little as 3 days led to a 10-fold reduction in engraftment effiency (Montarras et al., 2005). An even more marked reduction in transplantation linked to cell culture was observed in comparisons of cultured and freshly isolated canine muscle progenitor cells (Parker et al., 2012). Although the transplantation efficiency of muscle progenitors from model organisms has been enhanced previously by manipulation of Notch signaling (Parker et al., 2012) or substrate elasticity (Gilbert et al., 2010), there are no techniques currently for the expansion of self-renewing huSCs ex vivo.

Our limited understanding of huSC biology can be attributed in part to the difficulty of obtaining tissue samples and of isolating a pure population of huSCs (Boldrin et al., 2010). By comparison, techniques for the prospective isolation of mouse SCs have identified a well-defined myogenic SC population and have enabled extensive characterization of the molecular regulation of their quiescence, activation, and differentiation (Bosnakovski et al., 2008; Collins et al., 2005; Fukada et al., 2007; Liu et al., 2013; Montarras et al., 2005; Sherwood et al., 2004). Previous studies have used prospective isolation of mononuclear cell types with distinct surface protein expression to define subsets of myogenic and non-myogenic cells in human muscle. These studies have found that a myogenic population resides within cells expressing CD56 (NCAM) (Bareja et al., 2014; Pisani et al., 2010a, 2010b; Zheng et al., 2007). Zheng et al. have identified both $CD56^+CD34^-$ and $CD56^+CD34^+$ subsets with myogenic potential. The $CD56^+CD34^+$ subset is thought to represent a myoendothelial population with the capacity to differentiate into myogenic, chondrogenic, or osteogenic lineages (Zheng et al., 2007). A similar study of myogenic potential within muscle-resident human cell populations showed that a $CD56^+CD34^+$ population of bipotent progenitors can give rise to both myogenic and adipogenic cell types in vitro (Pisani et al., 2010a). In a second study, the same authors confirmed that both $CD56^+CD34^+$ and $CD56^+CD34^-$ cells have myogenic potential, but only the latter is restricted to a myogenic fate (Pisani et al., 2010b). More recently, Bareja et al. (2014) used CD34 as a negative selection marker for identification of a myogenic huSC within the $CD56^+$ population.

Thus, there remains a lack of consensus regarding the identity of huSCs and further studies are required to assess the myogenic identity of prospectively isolated populations at the resolution of single cells. Notably, previous prospective isolation studies assessed the myogenic potential of purified cell populations by the analysis of human-specific gene expression in engrafted muscle tissue, but did not study their stem cell potential by evaluating the self-renewal of these populations in vivo. Nonetheless, the dual potential for self-renewal and differentiation remains the defining feature of stem cells. Therefore, further characterization of the identity and stem cell characteristics of huSCs is essential for developing insight into their mechanisms of self-renewal.

To further our understanding of huSC biology, we used prospective cell isolation, RNA sequencing (RNA-seq) analyses, and cell transplantation to study a defined population of human myogenic progenitors with the potential to self-renew. This information was leveraged to identify changes in the molecular phenotype and self-renewal potential within the purified huSC population. Specifically, we mapped a core transcription factor regulatory network of self-renewal, and we established an essential role for p38 mitogen-activated protein kinase (MAPK) in the regulation of huSC regenerative capacity akin to that observed in mouse. Reversible pharmacologic inhibition of p38 in cultured huSCs resulted in a gene expression program consistent with the promotion of huSC self-renewal, and it allowed for expansion of a population of huSCs ex vivo with enhanced self-renewal and engraftment potential.

RESULTS

As the starting point of this study, we prospectively isolated huSCs from surgical specimens of skeletal muscle using fluorescence-activated cell sorting (FACS) to analyze cell-surface protein expression. To identify huSC surface markers, we sequentially screened known markers of mouse SCs and huSCs by analyzing extracellular protein expression in PAX7-expressing SCs associated with human muscle fiber explants (Figure S1A). Like mouse SCs, huSCs expressed β1-integrin (ITGB1), but did not express the endothelial marker CD31 or the hematopoietic marker CD45 (Sherwood et al., 2004). We observed that huSCs, in contrast to mouse SCs (Montarras et al., 2005; Sherwood et al., 2004), did not express detectable CD34. Furthermore, we found that the epidermal growth factor receptor (EGFR), which is expressed by mouse SCs (Golding et al., 2007) and exhibits a rapid decrease in expression early in the process of differentiation (Leroy et al., 2013), also was expressed by human fiber-associated SCs. Taken together, our studies defined huSCs as $CD34^-CD31^-CD45^-$ cells that can be further specified as a population that expresses ITGB1 and EGFR (Figures 1A and S1A). Using this surface protein signature, huSCs could be prospectively isolated from all muscles tested, including *latissimus dorsi*, *serratus anterior*, and *rectus abdominis* (Figure S1B).

To analyze the purity of cells within the putative huSC population, we quantified the percentage of cells expressing PAX7 (Figure 1B), which serves as a marker of huSCs. This analysis revealed that 96% ± 2% (n = 8) of cells in the huSC population express PAX7 (Figure 1B), while no PAX7-expressing cells were observed in the remaining huSC-depleted population, which consisted of all cells expressing CD34, CD31, or CD45 (Figure S1C). These data indicate that the sorting strategy highly enriches myogenic cells. As an additional analysis of the myogenic identity of the sorted cell populations, single-cell-derived clones were analyzed for expression of myogenic genes (Figure S1D). Although 100% of cells in the putative huSC-derived population yielded clones that expressed PAX7, no PAX7-expressing clones were derived from the remaining huSC-depleted cells. The myogenic identity of purified huSCs also was evaluated by analyzing the expression of a suite

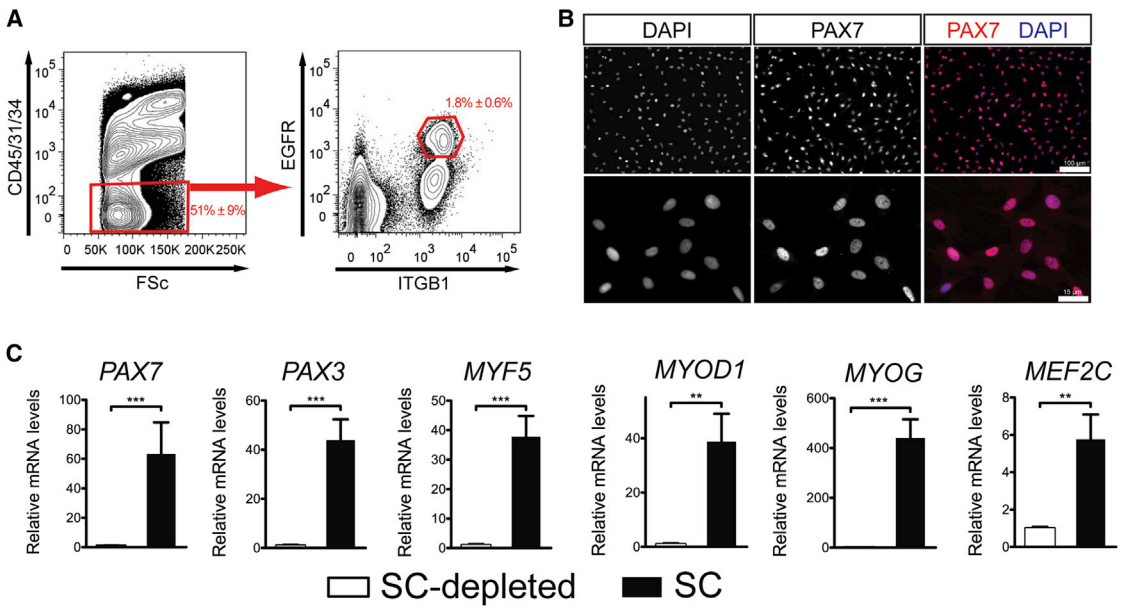

Figure 1. Identification and Prospective Isolation of HuSCs

(A) Cell-sorting scheme used to isolate huSCs by FACS for a representative specimen of *latissimus dorsi* muscle. Red gates indicate subpopulations containing huSCs. Numbers indicate percentage of total events falling within each gate; given error represents SD (n = 15).

(B) Immunofluorescence (IF) analysis of PAX7 expression in purified huSCs at low (top) and high (bottom) magnification 3 days after isolation. Cells were stained with antibodies against PAX7 and with DAPI to identify nuclei.

(C) qRT-PCR analysis of *PAX7*, *PAX3*, *MYF5*, *MYOD*, *MYOG*, and *MEF2C* mRNA levels in the huSC and huSC-depleted cell populations after a period of 7 days in culture is shown (n = 4). Error bars represent SD. *p < 0.05, **p < 0.01, ***p < 0.001.

of myogenic transcription factors relative to huSC-depleted cells (Figure 1C). In this analysis, cultured huSCs expressed significantly more *PAX7*, *PAX3*, *MYF5*, *MYOD*, *MYOG*, and *MEF2C* than the remaining huSC-depleted population. We also observed that a subset of activated huSC progeny fused to form multinucleate myotubes when cultured to ~90% confluency (Figure S1E). In contrast, the huSC-depleted population of cells grown under the same conditions did not exhibit signs of myogenesis in culture (Figure S1F), further indicating that the purification strategy efficiently enriches myogenic cells.

We next aimed to characterize changes in huSCs during ex vivo culture, which, in mice, results in a marked reduction in the capacity for tissue regeneration and self-renewal upon subsequent transplantation (Gilbert et al., 2010; Montarras et al., 2005). For this analysis, we used a basal culture medium supplemented with fetal bovine serum (FBS) and with insulin, transferrin, and selenium (Rocheteau et al., 2012). Additional specific growth factors were not included to limit perturbations that might confound the interpretation of stem cell behavior ex vivo. To study the behavior of huSCs during their growth in culture, we first used time-lapse microscopy to observe purified cells beginning shortly after prospective isolation. These real-time studies of huSCs revealed that, upon isolation, initially quiescent cells undergo a process of activation in which they initially grow in size and become motile (Movie S1). HuSCs first divided, on average, 83.3 ± 14.1 hr post-isolation (Figure S1G). Activated huSC progeny undergo a second cell division that occurs, on average, 25.5 ± 5.7 hr later (Figure S1H). Interestingly, the time to first cell division and the time between the first and second cell divisions were considerably longer for huSCs than for mouse SCs studied in similar conditions (Rodgers et al., 2014).

To further characterize the behavior of huSCs ex vivo, we maintained SC cultures and analyzed their growth over a period of 3 weeks. Cells were serially passaged to maintain cultures below 40% of confluency. In four independent cultures, we observed that freshly isolated cells underwent a period of exponential growth between ~4 and 9 days after isolation, typical of isolated murine SCs between ~3 and 5 days after isolation. After the exponential growth phase, the huSCs entered a phase of linear growth kinetics (Figure S1I), and this pattern persisted for the remainder of the observed period in culture. Thus, huSCs give rise to a pool of proliferating progeny in culture, which as a population exhibits a progressive slowing of the growth rate.

To study the molecular regulation of the phenotypic transition that occurs in activated huSCs, and as a resource for future studies of huSC-mediated myogenesis, we

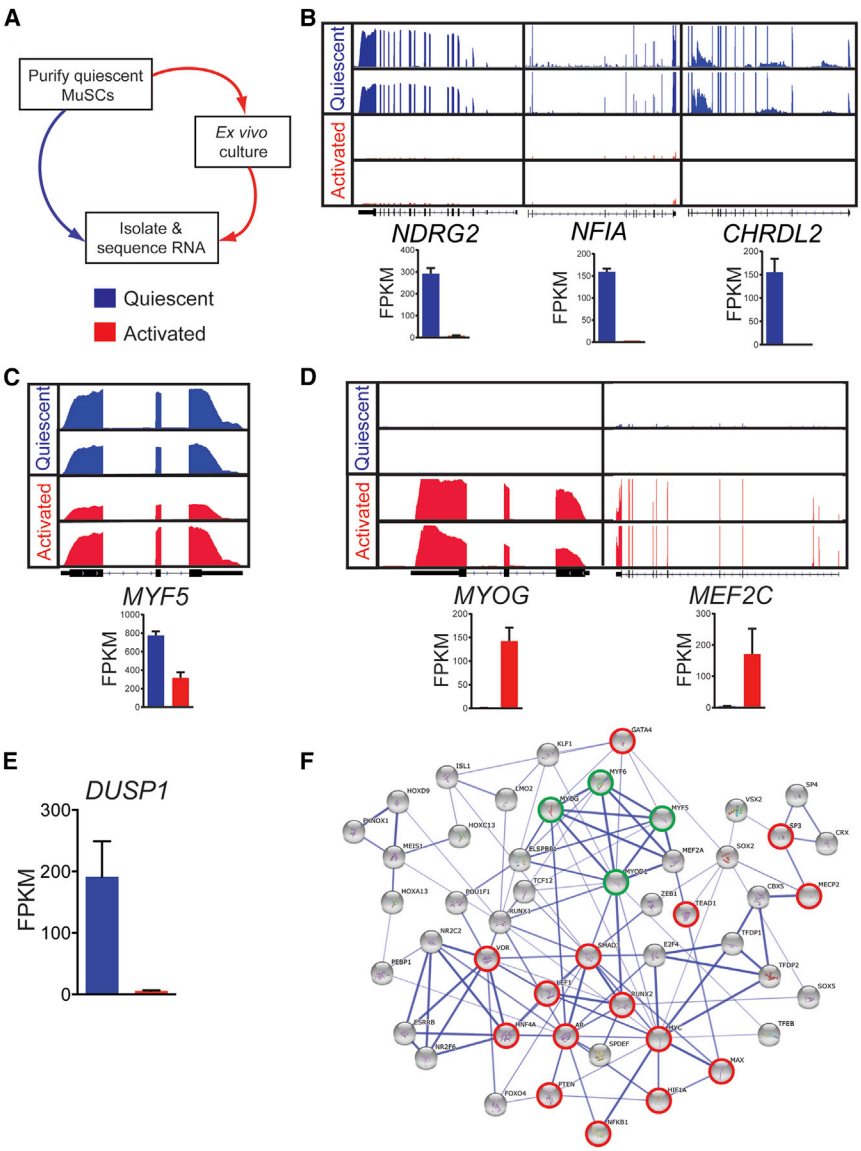

Figure 2. Transcriptome Profiles of Prospectively Isolated Quiescent and Activated HuSCs

(A) Schematic shows RNA-seq analysis of prospectively isolated quiescent and ex vivo activated huSCs.

(B) Representative RNA-seq analysis shows quiescent (blue) and activated (red) muscle SCs isolated from *latissimus dorsi* muscle.

(C) RNA-seq analysis shows *MYF5* expression in quiescent and activated huSCs.

(D) RNA-seq analysis shows expression of differentiation-associated transcription factors in quiescent and activated huSCs.

(E) Quantification of *DUSP1* expression in quiescent and activated huSCs based on RNA-seq analyses is shown.

(F) Transcription factor regulatory network of huSCs constructed from analysis of differential gene expression in quiescent and activated huSCs (see Experimental Procedures for details). Highlighted in red are transcription factors with known associations with the p38 MAPK signaling pathway; highlighted in green are myogenic regulatory factors. The strength of evidence for a given interaction is reflected by the hue of the edge connecting two nodes, with darker edges indicating greater confidence. For RNA-seq data, reads from two biological replicates per condition are shown mapped to the reference genome. The number of sequenced fragments per kilobase of exon per million fragments mapped (FPKM) in each condition is shown for individual genes (n = 2 biological replicates per condition). Error bars represent SD.

generated transcriptome profiles using RNA-seq of both freshly purified, quiescent huSCs and activated huSCs, the latter having been cultured for 7 days (Figure 2A). We chose to analyze cells following 7 days in culture in order to capture the population in a fully activated state, knowing that at 7 days the population of cultured huSCs is in a phase of exponential growth (Figure S1I) and the majority of cells in the population has undergone at least one division (Figures S1G and S1H; Movie S1). Relative to activated cells, freshly isolated quiescent huSCs express transcripts, such as *NFIA*, *NDRG2*, and *CHRDL2*, which also are expressed in quiescent, undifferentiated murine SCs (Fukada et al., 2007; Liu et al., 2013; Figure 2B). Quiescent huSCs also express high levels of *MYF5*, which decrease in activated huSCs (Figure 2C). Consistent with our previous characterizations of mouse SCs activated in response to injury in vivo (Liu et al., 2013), activated huSCs upregulated genes associated with cell proliferation and myogenic differentiation: unbiased analysis of the genes that exhibited greater than 10-fold increased expression in activated huSCs relative to quiescent huSCs revealed enrichment for genes associated with the mitotic cell cycle (gene ontology [GO]:0000278; $p = 6.5 \times 10^{-9}$) and muscle organ development (GO:0007517; $p = 1.5 \times 10^{-10}$). Furthermore, cultured huSCs expressed differentiation-associated transcription factors such as *MYOG* and *MEF2C* (Figure 2D). Cultured huSCs as a population also upregulated genes required for myofibril assembly and muscle contraction (e.g., *MYH3*, *CACNG1*, and *MYL2*) (Figure S2A), supporting the conclusion that activated huSCs initiate a

transcriptional program of myogenic differentiation even under high-mitogen growth conditions and sub-confluent cell density.

As an initial application of our RNA-seq datasets for discovery of regulatory mechanisms in huSCs, we compared transcriptomes of quiescent huSCs to those of activated huSCs to identify loci that were differentially expressed. In quiescent huSCs, we identified 998 highly expressed genes, including 133 loci annotated as transcription factors, 66 as receptors, and 56 as signaling molecules by the PANTHER gene ontology database (Table S1). Importantly, several known quiescent rodent SC-associated markers, such as *CALCR*, *CXCR4*, and *SPRY1*, were identified in this analysis, suggesting that the method was reliable in its identification of enriched transcripts. The same analysis of transcripts enriched in activated huSCs highlighted 708 transcripts, including 29 annotated transcription factors, 40 receptors, and 28 signaling molecules (Table S1). Here again we found many interesting and unanticipated transcripts and were reassured to find several known important regulators of myogenic differentiation, including *MYOD1*, *MYOG*, and *MEF2C*.

We further analyzed our transcriptional profiling data to computationally define biological processes over-represented among lists of differentially expressed genes. With this analysis, we identified a number of significantly enriched ($p < 0.05$) biological processes and their associated genes in both quiescent and activated huSCs (Tables S2 and S3). In activated huSCs, we identified hundreds of genes associated with muscle contraction, muscle development, mitosis, and the cell cycle, among other processes. In quiescent huSCs, we identified numerous genes linked to transcriptional regulation, signal transduction, and cell-cycle control. Of particular interest, several important components of the Notch signaling pathway were identified as differentially expressed genes in this analysis. The Notch signaling pathway is a regulator of various aspects of rodent SC quiescence and activation, and Notch transcriptional activity is required for the maintenance of quiescence in mouse SCs (Bjornson et al., 2012; Conboy and Rando, 2002; Mourikis et al., 2012). In cultured huSCs, we identified in particular downregulation of expression of the Notch receptor *NOTCH3* and of the canonical Notch target genes *HEY1*, *HEY2*, and *HES1* (Table S3), supporting the model arising from studies of mouse SCs that Notch signaling plays criticial roles in the function of undifferentiated muscle progenitors. These analyses suggest that networks of transcribed genes with specific roles in quiescent and activated huSCs can be efficiently identified within RNA-seq data.

To take further advantage of these RNA-seq datasets of huSCs, we sought to identify signaling pathways governing processes of proliferative expansion, self-renewal, and differentiation in order to seek genes and pathways whose manipulation might be valuable for therapeutic applications of prospectively isolated huSCs. Our analysis of transcription in huSCs revealed that, among the genes that are differentially expressed by activated huSCs relative to quiescent huSCs, genes associated with MAPK signaling are significantly enriched ($p = 1.2 \times 10^{-3}$). Among these genes, we noted a 35-fold decrease upon huSC activation in culture in the expression of *DUSP1* (Figure 2E), which encodes a dual-specificity phosphatase that dephosphorylates and, thus, inactivates p38 MAPK. This finding was of particular interest to us, given the implication of p38 MAPK signaling in the regulation of rodent muscle progenitor differentiation in the context of muscle regeneration (Lluís et al., 2006; Shi et al., 2010).

With our RNA-seq data, we constructed a core transcription factor network regulating the phenotypic changes upon culturing quiescent huSCs using published studies to identify relationships among known transcription factors that were computationally predicted to regulate genes that were differentially expressed by quiescent and activated huSCs (Figure 2F). In addition to the myogenic regulatory factors MYF5, MYOD1, MYOG, and MRF4, this network included a number of transcription factors regulated by p38, including HIF1A, PTEN, GATA4, SP3, SMAD3, NF-κB, VDR, AR, and MYC. To measure the extent of p38 activation in huSCs in vivo and in vitro, we analyzed the levels of phosphorylated (activated) p38 (p-p38). Although p-p38 was absent from quiescent SCs in histologic sections of human skeletal muscle, we observed robust p38 phosphorylation in activated huSCs in culture (Figure 3A). The activation of p38 in activated huSCs, as assessed by its phosphorylation, was independent of the density at which cells were cultured (Figures S2B and S2C). Taken together, these data support a model in which p38 MAPK is activated during ex vivo huSC growth, concurrent with a loss of proliferative potential and expression of differentiation-associated genes.

To determine whether the inhibition of p38 MAPK in activated huSCs could maintain their proliferative potential and prevent expression of genes for myogenic differentiation, we grew the cells in the presence of a small molecule p38 inhibitor (p38i; SB 203580) and analyzed both their transcriptional and functional properties. Though various p38 inhibitors have been developed, SB 203580 was selected for this study because its targeting specificity has been studied extensively (Cuenda and Cohen, 1999; Davies et al., 2000; Eyers et al., 1998; Gum et al., 1998). Given previous observations of dose-dependent cell growth inhibition by p38 inhibitors in transformed muscle progenitor cell lines (Jones et al., 2005), we first studied the effects of varying doses of p38 inhibitor on *PAX7* expression and cell proliferation in activated huSCs. *PAX7* expression, which is correlated with the

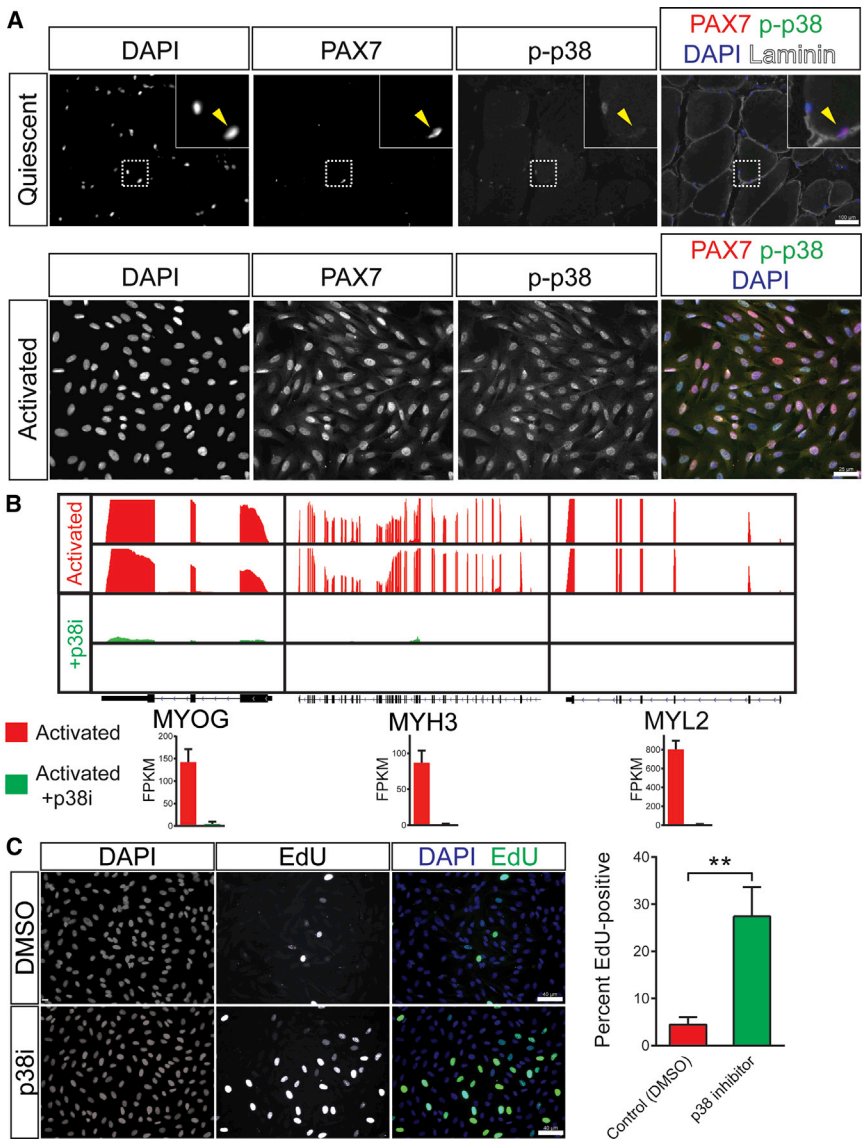

Figure 3. Regulation of p38 MAPK Signaling Controls HuSC Fate

(A) IF analysis shows activated p-p38 in quiescent huSCs in vivo (top) and activated huSCs ex vivo (bottom).

(B) RNA-seq analysis of markers of terminal differentiation in control untreated (red) and p38i-treated (green) activated huSCs. Sequencing reads from two biological replicates per condition are shown mapped to the reference genome. The FPKM in each condition is shown for individual genes (n = 2 biological replicates per condition).

(C) Representative fluorescence microscopy analysis of EdU incorporation in control and p38i-treated huSCs cultured for 9 days. The percentage of huSCs in each condition incorporating EdU during a 1-hr pulse was quantified (n = 4). Error bars represent SD. **p < 0.01.

undifferentiated muscle progenitor fate (Rocheteau et al., 2012), exhibited a dose-dependent increase as the concentration of p38i was increased from 0 to 10 μM, but did not significantly change at concentrations beyond 10 μM (Figure S3A). We next examined the effect of varying concentrations of p38i on the rate of proliferation of undifferentiated cells by analyzing huSCs cultured with or without inhibitor for only 3 days post-isolation. Although concentrations of p38i up to 10 μM showed equivalent rates of EdU incorporation, when cells were cultured with 20 μM p38i, the frequency of EdU incorporation was reduced significantly (Figure S3B). Because 10 μM p38i maximally induced expression of the stem cell marker *PAX7* without significantly limiting cell proliferation, this drug concentration was used for all subsequent studies of cell fate.

To test for effective inhibition of p38 activity in SC cultures treated with 10 μM p38i, we quantified the amount of p38 target protein phosphorylation in control and p38i-treated cultures. These studies revealed marked decreases in the levels of phosphorylation of two p38 substrates, phopsho-HSP27 (Ser82) (Larsen et al., 1997) and phospho-GYS1 (Ser645) (Kuma et al., 2004), in the presence of p38i (Figures S3C–S3F). Consistent with a model in which p38 activity prevents myogenic lineage progression, p38i-treated cells expressed levels of *MYOG*, *MYH3*, and *MYL2*, for example, that were significantly reduced in comparison to untreated cells (Figure 3B). We observed similar suppression of *MYOG* expression by SB 203580 and an alternative, specific p38 inhibitor, SB 239063, further supporting the conclusion that pharmacologic

manipulation of p38 in huSCs limits the expression of differentiation-associated genes (Figures S3G and S3H). Cells cultured in the presence of p38i also exhibited markedly diminished expression of MYOG and myosin heavy chain (MyHC) protein compared to controls (Figures S3I and S3J). Unbiased analysis of the set of genes that exhibited decreased expression due to p38i treatment revealed enrichment for genes associated with muscle contraction (GO:0006936; $p = 3.7 \times 10^{-15}$) and muscle organ development ($p = 2.2 \times 10^{-5}$). Although p38 inhibition blocked SC differentiation, we found that the expression of MYOD1 was not decreased in treated cells (Figure S3K), consistent with our findings in murine SCs of high levels of Myod1 expression in quiescent cells (Liu et al., 2013). The bulk of p38i-treated cultured huSCs also exhibited undiminished expression of the myogenic regulatory factor *MYF5* relative to untreated cells (Figure S3L). Pharmacologic inhibition of p38 MAPK signaling thus maintained cultured huSCs in an undifferentiated state ex vivo.

As a first test of the ability of p38 inhibition to maintain the proliferative potential of huSCs as undifferentiated cells, we measured the proliferation index of huSCs cultured in the presence or absence of p38i for 9 days by monitoring incorporation of EdU. While only 4.4% ± 0.4% of untreated cells incorporated EdU during a 1-hr pulse, 27% ± 2% of p38i-treated cells incorporated EdU (Figure 3C). Analysis of metaphase spreads of p38i-treated huSCs revealed normal chromosome number in 100% of cells after ten passages (Figure S3M). Consistent with the observation of increased EdU incorporation in p38i-treated huSCs after 9 days in culture, expression of genes associated with DNA replication and cell division, including *MKI67*, *NDC80*, *AURKB*, and *RFC4*, was increased in p38i-treated cells relative to untreated cells in the analyses of RNA-seq data (Figure S3N). Growth curves of p38i-treated huSCs maintained in culture for 3 weeks demonstrated preservation of exponential growth kinetics and massive expansion of the treated huSC cultures in comparison to parallel untreated control cultures from the same donor (Figure S3O). Thus, blocking huSC differentiation by inhibiting p38 maintains cells in an undifferentiated state in which they continued to proliferate without evidence of genetic instability.

Although inhibition of p38 MAPK signaling prevented spontaneous differentiation of huSCs ex vivo, this effect was reversible. After 2 weeks of expansion in the presence of p38i, the drug was chased for a period of 5 days, during which we observed a significant increase in *MYOG* expression (Figure S4A). After the 5-day chase, we also observed terminal differentiation of expanded cells into multinucleate MyHC-expressing myotubes (Figure S4B). These data indicate that the inhibition of huSC differentiation by p38i is reversible and that cells expanded with p38i retain the ability to terminally differentiate.

To test directly the self-renewal and tissue regenerative potential of expanded huSCs in vivo, we analyzed cell engraftment upon xenotransplantation into immunodeficient mice. As adult stem cells, huSCs are expected to yield progeny that either regenerate muscle tissue or replenish the pool of self-renewing stem cells. In transplantation studies, we compared the p38i-treated activated huSCs to two control cell populations as follows: (1) freshly isolated, uncultured quiescent huSCs; and (2) activated huSCs grown in the absence of p38i. We first tested huSC regenerative potential by analyzing the expression of human-specific nuclear lamin A/C (LMNA) and human-specific ITGB1 following transplantation of huSCs into *tibialis anterior* muscles. Expression of human/mouse laminin also was used to visualize gross muscle morphology. We observed robust engraftment of human LMNA-labeled nuclei that correlated with the expression of human ITGB1 in muscle fibers (Figures 4A and 4B; Figure S4C). The p38i-treated activated huSCs engrafted to form human ITGB1-expressing chimeric muscle fibers with approximately 4-fold and 11-fold greater efficiency than freshly isolated quiescent huSCs and control activated huSCs, respectively (221 ± 20 chimeric fibers per muscle cross-section from p38i-treated activated huSCs versus 49 ± 14 from quiescent huSCs and 21 ± 13 from untreated activated huSCs; $p < 0.001$ in separate comparisons of each control condition to the p38i-treated condition) (Figure 4A). Furthermore, human-mouse chimeric muscle fibers formed by the engraftment of p38i-expanded huSCs expressed human dystrophin (DMD) (Figure S4D). We also analyzed expanded huSC engraftment by studying fusion of huSCs engineered ex vivo by adenoviral infection to express a GFP transgene, giving rise to chimeric GFP-expressing muscle fibers in transplanted NSG mice (Figures S4E and S4F). These analyses demonstrate as a proof-of-concept that the prospectively isolated and expanded cells are genetically manipulable and capable of expressing donor-derived DMD in chimeric fibers.

To study the potential of transplanted huSCs to manifest a defining stem cell property by undergoing self-renewal to yield PAX7-expressing huSCs in vivo, we first examined the expression of PAX7 in nuclei of unfused human cells in recipient muscles. In this analysis, we observed PAX7-expressing nuclei of human origin that resided beneath the basal lamina (Figure 4B; Figures S4G and S4H). To compare quantitatively the potential of freshly isolated quiescent huSCs, control activated huSCs, and p38i-treated activated huSCs to engraft as mononuclear stem cells, we analyzed the abundance of unfused, donor human cells by flow cytometry. We initially confirmed that unfused donor cells expressed PAX7 as evidence that they had formed renewed

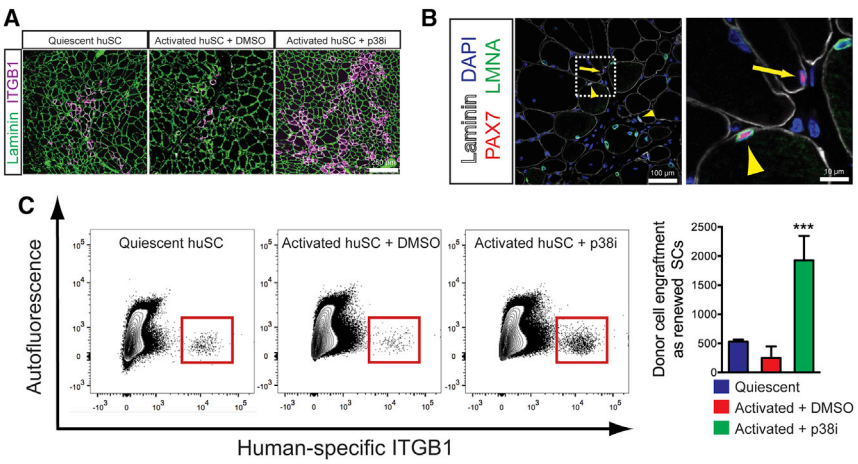

Figure 4. Xenotransplantation Reveals Regenerative Potential of Expanded HuSCs

(A) Four weeks after transplantation, engraftment of freshly isolated quiescent huSCs, control activated huSCs, and p38i-treated activated huSCs was determined by IF analysis of human-specific ITGB1 expression (magenta); 3 × 10^4 cells were used for each transplant. Anti-laminin (green) detects laminin of mouse and human origin.

(B) Representative low-magnification (left) and high-magnification (right) images of engrafted p38i-treated activated huSCs 4 weeks after transplantation into mouse muscle. The yellow arrowhead identifies a sublaminar PAX7-expressing cell of human origin; the yellow arrow identifies a nearby sublaminar Pax7-expressing cell of mouse origin.

(C) Representative flow cytometric analysis of human-specific ITGB1 expression in the bulk population of mononuclear cells isolated from mouse muscle transplanted with 3 × 10^4 huSCs per transplant. Quantification of total mononuclear human ITGB1-expressing cells per transplanted muscle revealed a 3.6-fold and 7.7-fold increase in engraftment of p38i-treated huSCs relative to quiescent huSCs and untreated activated huSCs, respectively. ***p < 0.001 comparing p38i-treated activated huSCs to control activated huSCs or quiescent huSCs (n = 4 per condition). Error bars represent SD.

huSCs (Figures S4I and S4J). Comparable to the analysis of fusion as an index of donor cell engraftment, p38i-treated activated huSCs had approximately 3.6-fold and 7.6-fold greater potential for engraftment as mononuclear SCs than quiescent huSCs and control activated huSCs, respectively (Figure 4C). Histological quantification of the number of human-derived, PAX7-expressing nuclei in cross-sections of transplanted muscle indicated a similar enhancement of engraftment by p38i-treated activated huSCs versus both quiescent huSCs and untreated activated huSCs. We, therefore, conclude that huSCs expanded in culture via p38 inhibition are capable of engrafting both as constituents of multinucleate muscle fibers and as self-renewed mononuclear huSCs.

The analysis of skeletal muscle regeneration and SC self-renewal following transplantation indicated that huSCs expanded in the presence of p38i exhibited tissue regenerative and self-renewal potential exceeding that of even freshly isolated quiescent huSCs. Given that quiescent huSCs are no more differentiated than p38i-treated cultured huSCs, the incongruent engraftment of these populations was surprising because it suggested that treating activated huSCs with p38i enhanced engraftment of the transplanted cells in part via a mechanism that was independent of blocking differentiation. We, therefore, sought to identify alternative mechanisms accounting for the enhanced self-renewal and tissue regenerative potential of p38i-treated huSCs using our RNA-seq analyses of these cell populations. In addition to the marked changes in gene expression noted previously (Figure 3; Table S4), we were intrigued to identify significant (p = 0.028) enrichment for genes associated with aging (GO:0007568) among the list of genes downregulated by p38 inhibition. This observation was particularly interesting in light of recent studies in which treatment of old mouse SCs with p38i was observed to rejuvenate aspects of their regenerative function, including their potential to regenerate damaged muscle following transplantation (Bernet et al., 2014; Cosgrove et al., 2014). We discovered six aging-associated genes with decreased expression in p38i-treated relative to untreated cultured huSCs: *LIMS1*, *CRYAB*, *ENG*, *ENO3*, *LRP1*, and *SERPINE1*. Of these, expression of *CRYAB*, *ENG*, *LRP1*, and *SERPINE1* also was reduced by more than 50% in p38i-treated huSCs relative to quiescent huSCs. Based on these unbiased analyses of genome expression data, we propose that these genes in particular may function as important regulators of huSC self-renewal downstream of p38.

DISCUSSION

In this study, we used a unique profile of surface markers to identify and prospectively isolate huSCs from surgical specimens. Importantly, these markers were observed to be expressed in situ by huSCs associated with whole human skeletal muscle fibers. Additionally, the marker profile used in this study was able to prospectively identify huSCs from each of three different muscles analyzed and from subjects of various ages. These markers, therefore, represent a reproducible and broadly applicable signature of huSCs. Additional analysis of huSC markers may allow simplification of the sorting strategy presented here. For instance, CD31

may redundantly identify CD34-expressing endothelial cells and may not be necessary to isolate a pure population of huSCs. As in previous studies (Bareja et al., 2014; Pisani et al., 2010b), we found that the predominant myogenic population did not express CD34. In contrast to previous studies, however, we found little evidence for a second myogenic population within the CD34-expressing cell population. Analysis of myogenic marker expression in single cells and clones revealed an absence of spontaneous myogenic activity within $CD34^+$ cells. Future studies are required to determine what technical variables account for differences in the characterization of the myogenic potential of CD34-expressing progenitors in human muscle.

We report an RNA-seq-based characterization of huSCs, including prospectively isolated quiescent huSCs analyzed immediately after sorting. A number of observations stemming from our studies support the characterization of these cells as quiescent. Most notably, these cells were nondividing upon isolation, as clearly manifested in our time-lapse microscopy studies. Indeed, although the isolation and culture in high-mitogen conditions induces these cells to activate, the huSCs typically did not undergo their first division until after more than 3 days in culture. The RNA-seq data provide additional confirmation of the quiescent nature of the prospectively isolated huSCs, which expressed low levels of numerous proliferation-related genes relative to the cultured huSCs. That these purified huSCs are functionally quiescent is not to say that they are *identical* to the huSCs in vivo. In fact, we know that the process of isolating the cells, which takes 5–6 hr on average and involves physical and enzymatic perturbations of the cell and its environment, is enough to induce biochemical changes within the huSCs. The extent of these differences, however, is difficult to assess given that the most thorough characterizations of the cells, such as RNA-seq, obviously cannot be performed on cells in vivo. Still, we know from several studies of SC quiescence in mouse that characterizations of FACS-purified cells can offer insight into the biology of SC quiescence in vivo (Cheung et al., 2012; Hausburg et al., 2015; Liu et al., 2013; Rodgers et al., 2014).

These studies add to a growing body of information related to the role of p38 MAPK signaling in skeletal muscle progenitor cells. Over a decade ago, a requirement for p38 in the regulation of rodent myoblast differentiation was defined (Cuenda and Cohen, 1999; Zetser et al., 1999). Based on these prior studies, the functions of p38 MAPK are clearly diverse and complex. p38 activation correlates with rodent SC activation, and pharmacologic inhibition of p38α/β can promote muscle progenitor cell-cycle exit (Jones et al., 2005). Intriguingly, and somewhat paradoxically, genetic absence of p38α, the dominant p38 isoform regulating the myogenic program in mice (Lovett et al., 2010), enhances proliferative expansion of the murine SC population postnatally and in response to injury, although p38α is not absolutely required for myogenic differentiation in vivo (Brien et al., 2013). That the p38α isoform is not required for differentiation may be due to redundant functions of p38β or ɣ isoforms, both of which are expressed in muscle and are capable of independently regulating muscle progenitor differentiation (Wang et al., 2008). Our studies suggest that, in humans, there is a switch that occurs in the activation of p38 as SCs are activated in culture, akin to the activation of p38 observed in mouse (Jones et al., 2005), going from an inactive unphosphorylated form in quiescent huSCs to an active phosphorylated form in cultured huSCs. Altogether, our data and previously published studies of p38 in rodent muscle progentiors support a model in which inhibition of p38 activity promotes exponential growth of progenitors by maintaining an undifferentiated fate. This model seems to be conserved between mice and humans. We further demonstrate that pharmacologic manipulation of p38 signaling can be leveraged for enhancement of both ex vivo expansion and subsequent in vivo engraftment of huSCs.

In our investigation, transplantation of huSCs expanded in the presence of p38i, generated more chimeric muscle fibers, and self-renewed huSCs in comparison to freshly isolated cells. What might account for the enhanced regenerative potential of expanded huSCs? One possibility is that the activated state of expanded cells relative to quiescent cells enabled the expanded cells to proliferate more during the course of muscle regeneration. In previous studies of cultured mouse SCs, this phenomenon may not have manifested as efficient engraftment because activation coincided with differentiation. By divorcing SC activation from differentiation, p38 inhibition may have revealed an increased engraftment potential of activated relative to quiescent cells. This possibility is particularly interesting given that we observed slower activation kinetics in purified huSCs relative to what has been reported for their mouse counterparts (Rodgers et al., 2014). An alternative explanation for the enhanced regenerative potential of the expanded huSCs is that p38 inhibition induces an epigenetic change in the cultured cells that promotes their engraftment potential. This hypothesis may relate to recent observations in aforementioned studies of mouse SCs, which showed an improved function in aged mouse SCs following treatment with a p38 inhibitor (Bernet et al., 2014; Cosgrove et al., 2014). The huSCs used in our study were isolated from donors with an age that greatly exceeds that of even aged mice. It is, therefore, plausible that human adult SCs exhibit a favorable response to treatment with p38i analogous to that observed in SCs from aged mice.

Although the mechanisms of this epigenetic restoration of SC function have not been elucidated, our analysis of

the gene expression changes stimulated by p38 inhibition identified several intriguing candidate regulators, including *ENG*, *CRYAB*, and *SERPINE1*. Our current understanding of the functions of these proteins suggests a plausible role for each in the aging of huSCs. *ENG* encodes endoglin, a membrane glycoprotein important in TGF-β signal transduction (Cheifetz et al., 1992). Increased expression of endoglin has been associated with aging phenotypes within endothelial and myeloid lineages (Aristorena et al., 2014; Blanco and Bernabeu, 2011), and excessive TGF-β signaling has been linked to impaired self-renewal of mouse SCs in the context of aging and chronic disease (Biressi et al., 2014; Carlson et al., 2008). Alpha-crystallin B chain (*CRYAB*) is a small heat shock protein, decreased expression of which has been linked to improved outcomes following cardiac ischemia in aged mice (Benjamin et al., 2007). *SERPINE1*, also known as plasminogen activator inhibitor-1 (PAI-1), is upregulated in senescent human cells and in various tissues of progeroid mouse models, including skeletal muscle (Baker et al., 2011; Mu and Higgins, 1995). Remarkably, genetic or pharmacologic inhibition of PAI-1 has been shown to improve organ function and extend the lifespan of progeroid mice (Eren et al., 2014). Future studies will be important to define the specific role of these genes during aging and muscle regeneration as regulators of huSCs downstream of p38 MAPK signaling.

EXPERIMENTAL PROCEDURES

Human Skeletal Muscle Specimens

Surgical specimens of human skeletal muscle were isolated in accordance with the Stanford Institutional Review Board. All experiments, unless otherwise noted, were performed using specimens of *latissimus dorsi* muscle. Additional details are included in the Supplemental Experimental Procedures.

HuSC Isolation

Human skeletal muscle tissue was first minced and incubated in collagenase II (750 U/ml, Worthington Biochemical) in Ham's F10 medium supplemented with 10% horse serum (Invitrogen) and 1% penicillin-streptomycin (Omega Scientific) at 37°C for 90 min in a shaking water bath (60 rpm). The digested muscle was washed in F10 with 10% horse serum and digested further in a shaking water bath at 37°C for 30 min in collagenase II (100 U/ml) and dispase (2 U/ml, Gibco) in F10 with 10% horse serum. Subsequent steps in the isolation procedure are detailed in the Supplemental Experimental Procedures.

Human Muscle Fiber Explants and Immunofluorescence Analysis

Human skeletal muscle specimens were incubated in collagenase (500 U/ml) in Ham's F10 supplemented with 10% horse serum and 1% penicillin-streptomycin for 80 min in a shaking water bath. Tissue was then triturated with a glass Pasteur pipet to separate single muscle fibers. Additional details are included in the Supplemental Experimental Procedures.

HuSC Culture

Slides or plates were coated with extracellular matrix protein (ECM, Sigma) at a concentration of 1:500 (v/v) in DMEM with 1% penicillin-streptomycin. Culture medium was a 1:1 mixture of DMEM:MCDB supplemented with 20% FBS (Omega Scientific), 1% insulin-transferrin-selenium (ITS, Invitrogen), and 1% penicillin-streptomycin. Four serum lots from two manufacturers (Omega Scientific and Atlanta Biologicals) were tested in assays of huSC growth and differentiation. Additional protocols for SC culture are presented in the Supplemental Experimental Procedures.

qRT-PCR

Freshly isolated huSCs or huSC-depleted cells were cultured for 7 days prior to analysis. For RNA isolation, cells were first rinsed twice in PBS. Cells were then lysed and RNA was isolated using an RNeasy Mini Kit (QIAGEN) according to the manufacturer's instructions. Additional details are described in the Supplemental Experimental Procedures.

Statistical Analysis

All statistical tests, except those involving gene set enrichment analyses, were unpaired, two-tailed t tests performed using GraphPad Prism 6.0. All error bars represent SDs, unless otherwise noted. Data from each experiment represent statistics compiled from true biological replicates, defined here as experiments performed with similar, but entirely unique, biological reagents. In the context of the human studies presented here, including the RNA-seq analyses, replicate experiments were always performed using cells from distinct donors.

ACCESSION NUMBERS

The accession number for the RNA-seq data reported in this paper is European Nucleotide Archive (ENA): PRJEB10091 (http://www.ebi.ac.uk/ena/data/view/PRJEB10091).

SUPPLEMENTAL INFORMATION

Supplemental Information includes Supplemental Experimental Procedures, four figures, four tables, and one movie and can be found with this article online at http://dx.doi.org/10.1016/j.stemcr.2015.08.004.

ACKNOWLEDGMENTS

The authors gratefully acknowledge the assistance of Amanda Khuong in the Department of Cardiothoracic Surgery and of Ziming Weng, Keith Bettinger, and Nathan Hammond at the Stanford Center for Genomics and Personalized Medicine. This work was supported by the Glenn Foundation for Medical Research, fellowships from the NIH (F30 AG035521), and Stanford University School of Medicine Medical Scientist Training Program to G.W.C.; by grants from the Department of Veterans Affairs (Merit

Review) to J.B.S.; and by grants from the Department of Veterans Affairs (Merit Review) and the NIH (P01 AG036695, R37 AG23806, and R01 AR062185) to T.A.R.

Received: December 8, 2014
Revised: August 5, 2015
Accepted: August 5, 2015
Published: September 3, 2015

REFERENCES

Aristorena, M., Blanco, F.J., de Las Casas-Engel, M., Ojeda-Fernandez, L., Gallardo-Vara, E., Corbi, A., Botella, L.M., and Bernabeu, C. (2014). Expression of endoglin isoforms in the myeloid lineage and their role during aging and macrophage polarization. J. Cell Sci. *127*, 2723–2735.

Baker, D.J., Wijshake, T., Tchkonia, T., LeBrasseur, N.K., Childs, B.G., van de Sluis, B., Kirkland, J.L., and van Deursen, J.M. (2011). Clearance of p16Ink4a-positive senescent cells delays ageing-associated disorders. Nature *479*, 232–236.

Bareja, A., Holt, J.A., Luo, G., Chang, C., Lin, J., Hinken, A.C., Freudenberg, J.M., Kraus, W.E., Evans, W.J., and Billin, A.N. (2014). Human and mouse skeletal muscle stem cells: convergent and divergent mechanisms of myogenesis. PLoS ONE *9*, e90398.

Benjamin, I.J., Guo, Y., Srinivasan, S., Boudina, S., Taylor, R.P., Rajasekaran, N.S., Gottlieb, R., Wawrousek, E.F., Abel, E.D., and Bolli, R. (2007). CRYAB and HSPB2 deficiency alters cardiac metabolism and paradoxically confers protection against myocardial ischemia in aging mice. Am. J. Physiol. Heart Circ. Physiol. *293*, H3201–H3209.

Bernet, J.D., Doles, J.D., Hall, J.K., Kelly Tanaka, K., Carter, T.A., and Olwin, B.B. (2014). p38 MAPK signaling underlies a cell-autonomous loss of stem cell self-renewal in skeletal muscle of aged mice. Nat. Med. *20*, 265–271.

Biressi, S., Miyabara, E.H., Gopinath, S.D., Carlig, P.M.M., and Rando, T.A. (2014). A Wnt-TGFβ2 axis induces a fibrogenic program in muscle stem cells from dystrophic mice. Sci. Transl. Med. *6*, 267ra176.

Bjornson, C.R.R., Cheung, T.H., Liu, L., Tripathi, P.V., Steeper, K.M., and Rando, T.A. (2012). Notch signaling is necessary to maintain quiescence in adult muscle stem cells. Stem Cells *30*, 232–242.

Blanco, F.J., and Bernabeu, C. (2011). Alternative splicing factor or splicing factor-2 plays a key role in intron retention of the endoglin gene during endothelial senescence. Aging Cell *10*, 896–907.

Boldrin, L., Muntoni, F., and Morgan, J.E. (2010). Are human and mouse satellite cells really the same? J. Histochem. Cytochem. *58*, 941–955.

Bosnakovski, D., Xu, Z., Li, W., Thet, S., Cleaver, O., Perlingeiro, R.C.R., and Kyba, M. (2008). Prospective isolation of skeletal muscle stem cells with a Pax7 reporter. Stem Cells *26*, 3194–3204.

Brien, P., Pugazhendhi, D., Woodhouse, S., Oxley, D., and Pell, J.M. (2013). p38α MAPK regulates adult muscle stem cell fate by restricting progenitor proliferation during postnatal growth and repair. Stem Cells *31*, 1597–1610.

Carlson, M.E., Hsu, M., and Conboy, I.M. (2008). Imbalance between pSmad3 and Notch induces CDK inhibitors in old muscle stem cells. Nature *454*, 528–532.

Cheifetz, S., Bellón, T., Calés, C., Vera, S., Bernabeu, C., Massagué, J., and Letarte, M. (1992). Endoglin is a component of the transforming growth factor-beta receptor system in human endothelial cells. J. Biol. Chem. *267*, 19027–19030.

Cheung, T.H., Quach, N.L., Charville, G.W., Liu, L., Park, L., Edalati, A., Yoo, B., Hoang, P., and Rando, T.A. (2012). Maintenance of muscle stem-cell quiescence by microRNA-489. Nature *482*, 524–528.

Collins, C.A., Olsen, I., Zammit, P.S., Heslop, L., Petrie, A., Partridge, T.A., and Morgan, J.E. (2005). Stem cell function, self-renewal, and behavioral heterogeneity of cells from the adult muscle satellite cell niche. Cell *122*, 289–301.

Conboy, I.M., and Rando, T.A. (2002). The regulation of Notch signaling controls satellite cell activation and cell fate determination in postnatal myogenesis. Dev. Cell *3*, 397–409.

Cosgrove, B.D., Gilbert, P.M., Porpiglia, E., Mourkioti, F., Lee, S.P., Corbel, S.Y., Llewellyn, M.E., Delp, S.L., and Blau, H.M. (2014). Rejuvenation of the muscle stem cell population restores strength to injured aged muscles. Nat. Med. *20*, 255–264.

Cuenda, A., and Cohen, P. (1999). Stress-activated protein kinase-2/p38 and a rapamycin-sensitive pathway are required for C2C12 myogenesis. J. Biol. Chem. *274*, 4341–4346.

Davies, S.P., Reddy, H., Caivano, M., and Cohen, P. (2000). Specificity and mechanism of action of some commonly used protein kinase inhibitors. Biochem. J. *351*, 95–105.

Eren, M., Boe, A.E., Murphy, S.B., Place, A.T., Nagpal, V., Morales-Nebreda, L., Urich, D., Quaggin, S.E., Budinger, G.R.S., Mutlu, G.M., et al. (2014). PAI-1-regulated extracellular proteolysis governs senescence and survival in Klotho mice. Proc. Natl. Acad. Sci. USA *111*, 7090–7095.

Eyers, P.A., Craxton, M., Morrice, N., Cohen, P., and Goedert, M. (1998). Conversion of SB 203580-insensitive MAP kinase family members to drug-sensitive forms by a single amino-acid substitution. Chem. Biol. *5*, 321–328.

Fukada, S., Uezumi, A., Ikemoto, M., Masuda, S., Segawa, M., Tanimura, N., Yamamoto, H., Miyagoe-Suzuki, Y., and Takeda, S. (2007). Molecular signature of quiescent satellite cells in adult skeletal muscle. Stem Cells *25*, 2448–2459.

Gilbert, P.M., Havenstrite, K.L., Magnusson, K.E.G., Sacco, A., Leonardi, N.A., Kraft, P., Nguyen, N.K., Thrun, S., Lutolf, M.P., and Blau, H.M. (2010). Substrate elasticity regulates skeletal muscle stem cell self-renewal in culture. Science *329*, 1078–1081.

Golding, J.P., Calderbank, E., Partridge, T.A., and Beauchamp, J.R. (2007). Skeletal muscle stem cells express anti-apoptotic ErbB receptors during activation from quiescence. Exp. Cell Res. *313*, 341–356.

Gum, R.J., McLaughlin, M.M., Kumar, S., Wang, Z., Bower, M.J., Lee, J.C., Adams, J.L., Livi, G.P., Goldsmith, E.J., and Young, P.R. (1998). Acquisition of sensitivity of stress-activated protein kinases to the p38 inhibitor, SB 203580, by alteration of one or more amino acids within the ATP binding pocket. J. Biol. Chem. *273*, 15605–15610.

Hall, J.K., Banks, G.B., Chamberlain, J.S., and Olwin, B.B. (2010). Prevention of muscle aging by myofiber-associated satellite cell transplantation. Sci. Transl. Med. *2*, 57ra83.

Hausburg, M.A., Doles, J.D., Clement, S.L., Cadwallader, A.B., Hall, M.N., Blackshear, P.J., Lykke-Andersen, J., and Olwin, B.B. (2015). Post-transcriptional regulation of satellite cell quiescence by TTP-mediated mRNA decay. eLife *4*, e03390.

Jones, N.C., Tyner, K.J., Nibarger, L., Stanley, H.M., Cornelison, D.D.W., Fedorov, Y.V., and Olwin, B.B. (2005). The p38α/β MAPK functions as a molecular switch to activate the quiescent satellite cell. J. Cell Biol. *169*, 105–116.

Karpati, G., Pouliot, Y., Zubrzycka-Gaarn, E., Carpenter, S., Ray, P.N., Worton, R.G., and Holland, P. (1989). Dystrophin is expressed in mdx skeletal muscle fibers after normal myoblast implantation. Am. J. Pathol. *135*, 27–32.

Kuma, Y., Campbell, D.G., and Cuenda, A. (2004). Identification of glycogen synthase as a new substrate for stress-activated protein kinase 2b/p38beta. Biochem. J. *379*, 133–139.

Larsen, J.K., Yamboliev, I.A., Weber, L.A., and Gerthoffer, W.T. (1997). Phosphorylation of the 27-kDa heat shock protein via p38 MAP kinase and MAPKAP kinase in smooth muscle. Am. J. Physiol. *273*, L930–L940.

Leroy, M.C., Perroud, J., Darbellay, B., Bernheim, L., and Konig, S. (2013). Epidermal growth factor receptor down-regulation triggers human myoblast differentiation. PLoS ONE *8*, e71770.

Liu, L., Cheung, T.H., Charville, G.W., Hurgo, B.M.C., Leavitt, T., Shih, J., Brunet, A., and Rando, T.A. (2013). Chromatin modifications as determinants of muscle stem cell quiescence and chronological aging. Cell Rep. *4*, 189–204.

Lluís, F., Perdiguero, E., Nebreda, A.R., and Muñoz-Cánoves, P. (2006). Regulation of skeletal muscle gene expression by p38 MAP kinases. Trends Cell Biol. *16*, 36–44.

Lovett, F.A., Cosgrove, R.A., Gonzalez, I., and Pell, J.M. (2010). Essential role for p38alpha MAPK but not p38gamma MAPK in Igf2 expression and myoblast differentiation. Endocrinology *151*, 4368–4380.

Mauro, A. (1961). Satellite cell of skeletal muscle fibers. J. Biophys. Biochem. Cytol. *9*, 493–495.

Montarras, D., Morgan, J., Collins, C., Relaix, F., Zaffran, S., Cumano, A., Partridge, T., and Buckingham, M. (2005). Direct isolation of satellite cells for skeletal muscle regeneration. Science *309*, 2064–2067.

Mourikis, P., Sambasivan, R., Castel, D., Rocheteau, P., Bizzarro, V., and Tajbakhsh, S. (2012). A critical requirement for notch signaling in maintenance of the quiescent skeletal muscle stem cell state. Stem Cells *30*, 243–252.

Mu, X.C., and Higgins, P.J. (1995). Differential growth state-dependent regulation of plasminogen activator inhibitor type-1 expression in senescent IMR-90 human diploid fibroblasts. J. Cell. Physiol. *165*, 647–657.

Parker, M.H., Loretz, C., Tyler, A.E., Duddy, W.J., Hall, J.K., Olwin, B.B., Bernstein, I.D., Storb, R., and Tapscott, S.J. (2012). Activation of Notch signaling during ex vivo expansion maintains donor muscle cell engraftment. Stem Cells *30*, 2212–2220.

Partridge, T.A., Morgan, J.E., Coulton, G.R., Hoffman, E.P., and Kunkel, L.M. (1989). Conversion of mdx myofibres from dystrophin-negative to -positive by injection of normal myoblasts. Nature *337*, 176–179.

Pisani, D.F., Clement, N., Loubat, A., Plaisant, M., Sacconi, S., Kurzenne, J.-Y., Desnuelle, C., Dani, C., and Dechesne, C.A. (2010a). Hierarchization of myogenic and adipogenic progenitors within human skeletal muscle. Stem Cells *28*, 2182–2194.

Pisani, D.F., Dechesne, C.A., Sacconi, S., Delplace, S., Belmonte, N., Cochet, O., Clement, N., Wdziekonski, B., Villageois, A.P., Butori, C., et al. (2010b). Isolation of a highly myogenic CD34-negative subset of human skeletal muscle cells free of adipogenic potential. Stem Cells *28*, 753–764.

Rocheteau, P., Gayraud-Morel, B., Siegl-Cachedenier, I., Blasco, M.A., and Tajbakhsh, S. (2012). A subpopulation of adult skeletal muscle stem cells retains all template DNA strands after cell division. Cell *148*, 112–125.

Rodgers, J.T., King, K.Y., Brett, J.O., Cromie, M.J., Charville, G.W., Maguire, K.K., Brunson, C., Mastey, N., Liu, L., Tsai, C.-R., et al. (2014). mTORC1 controls the adaptive transition of quiescent stem cells from G0 to G(Alert). Nature *510*, 393–396.

Sacco, A., Doyonnas, R., Kraft, P., Vitorovic, S., and Blau, H.M. (2008). Self-renewal and expansion of single transplanted muscle stem cells. Nature *456*, 502–506.

Sherwood, R.I., Christensen, J.L., Conboy, I.M., Conboy, M.J., Rando, T.A., Weissman, I.L., and Wagers, A.J. (2004). Isolation of adult mouse myogenic progenitors: functional heterogeneity of cells within and engrafting skeletal muscle. Cell *119*, 543–554.

Shi, H., Boadu, E., Mercan, F., Le, A.M., Flach, R.J.R., Zhang, L., Tyner, K.J., Olwin, B.B., and Bennett, A.M. (2010). MAP kinase phosphatase-1 deficiency impairs skeletal muscle regeneration and exacerbates muscular dystrophy. FASEB J. *24*, 2985–2997.

Snow, M.H. (1978). An autoradiographic study of satellite cell differentiation into regenerating myotubes following transplantation of muscles in young rats. Cell Tissue Res. *186*, 535–540.

Wang, H., Xu, Q., Xiao, F., Jiang, Y., and Wu, Z. (2008). Involvement of the p38 mitogen-activated protein kinase α, β, and γ isoforms in myogenic differentiation. Mol. Biol. Cell *19*, 1519–1528.

Zetser, A., Gredinger, E., and Bengal, E. (1999). p38 mitogen-activated protein kinase pathway promotes skeletal muscle differentiation. Participation of the Mef2c transcription factor. J. Biol. Chem. *274*, 5193–5200.

Zheng, B., Cao, B., Crisan, M., Sun, B., Li, G., Logar, A., Yap, S., Pollett, J.B., Drowley, L., Cassino, T., et al. (2007). Prospective identification of myogenic endothelial cells in human skeletal muscle. Nat. Biotechnol. *25*, 1025–1034.

Stem Cell Reports, Volume *5*

Supplemental Information

Ex Vivo Expansion and In Vivo Self-Renewal of Human Muscle Stem Cells

Gregory W. Charville, Tom H. Cheung, Bryan Yoo, Pauline J. Santos, Gordon K. Lee, Joseph B. Shrager, and Thomas A. Rando

SUPPLEMENTAL FIGURES

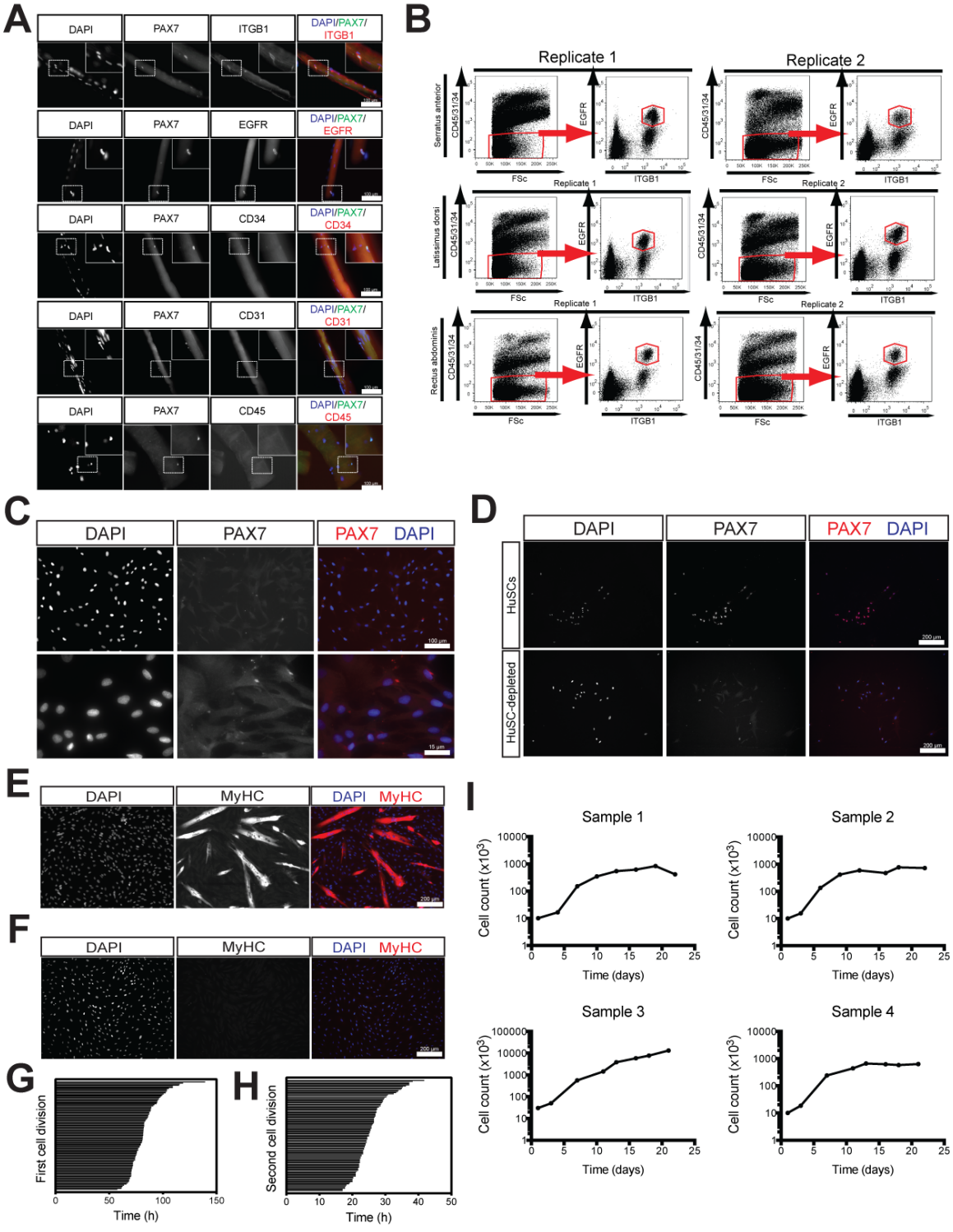

Figure S1. **Characteristics of prospectively isolated huSCs. Related to Figure 1. (A)** Immunofluorescence (IF) analysis of PAX7 and surface protein expression in huSCs in association with intact explanted human muscle fibers. Nuclei were stained with DAPI. Insets are magnified views of MuSCs in each image. **(B)** Representative FACS plots for prospective isolation of human huSCs from *serratus anterior*, *latissimus dorsi*, and *rectus abdominis* muscles. Cells were gated by forward scatter and side scatter (not shown) prior to gating for CD45/31/34, EGFR, and ITGB1. The populations containing huSCs are highlighted in red. Two biological replicates (Replicates 1 and 2) are shown for each muscle. **(C)** IF analysis of PAX7 expression in huSC-depleted cells cultured for 3 days. Representative images are shown at low (top) and high (bottom) magnification. **(D)** Representative IF analysis of a PAX7-expressing clone derived from the huSC subpopulation (left) and a clone derived from the huSC-depleted subpopulation (right) in which no PAX7 expression was observed. Nuclei were stained with DAPI. **(E)** IF analysis of MyHC expression in huSCs cultured for 9 days up to ~90% of confluency. Nuclei were stained with DAPI. **(F)** Single-color IF analysis of MyHC expression in cells from the huSC-depleted subpopulation cultured for 9 days up to ~90% of confluency. Nuclei were stained with DAPI. **(G)** Time from plating to first cell division of 100 freshly isolated huSCs from three biological replicates as determined by time-lapse microscopy. Each horizontal bar represents a single cell. The length of a given bar along the x-axis reflects the length of time required to reach the first cell division (83.3 ± 14.1 h, $n = 200$ cells from four biological replicates). Bars are ordered along y-axis by length of cell cycle (longest at the top). **(H)** Time between first and second cell division of 100 freshly isolated huSCs from three biological replicates as determined by time-lapse microscopy.

The length of a given bar along the x-axis reflects the length of time between the first and second cell divisions (25.5 ± 5.7 h, n = 200 cells from four biological replicates). Bars are ordered along y-axis by length of cell cycle (longest at the top). **(I)** Growth curves of huSCs isolated from four biological replicates (unique clinical specimens). Cells were serially passaged to maintain a density of <40% confluency and were counted at each passage.

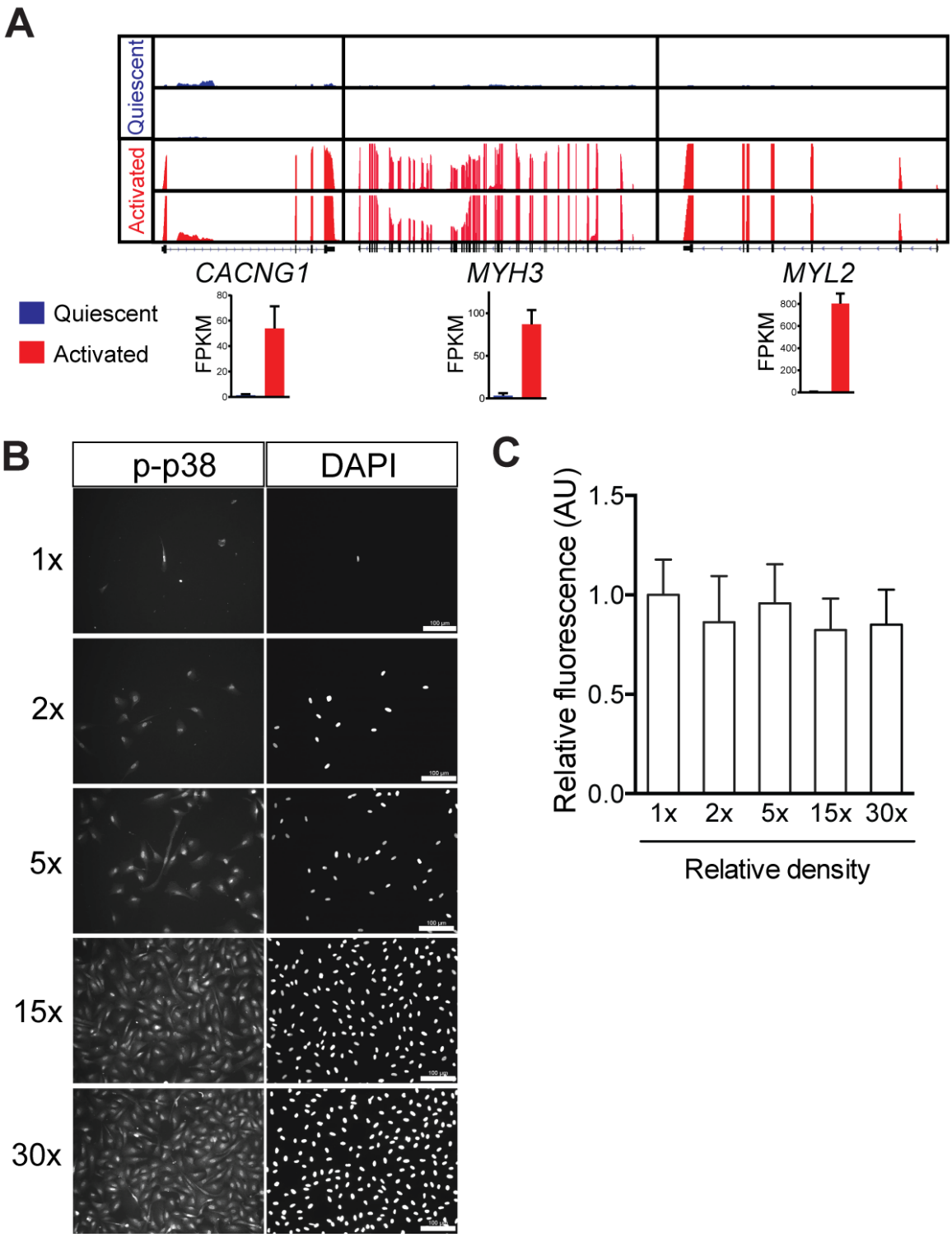
A
Quiescent
Activated
CACNG1
MYH3
MYL2
FPKM
Quiescent
Activated
B
p-p38
DAPI
1x
2x
5x
15x
30x
C
Relative fluorescence (AU)
1.5
1.0
0.5
0.0
1x
2x
5x
15x
30x
Relative density

Figure S2. Terminal differentiation of huSCs and effects of cell density on p38 activity. Related to Figure 2. (A) Shown are sequencing reads from 2 biological replicates per condition (quiescent and activated) mapped to the reference genome. The number of sequenced fragments per kilobase of exon per million fragments mapped (FPKM) in each condition is shown for individual genes. Error bars represent standard deviation. **(B)** Representative IF analysis of p-p38 in huSCs cultured for 5 days at the given relative density. **(C)** Quantification of nuclear p-p38 fluorescence intensity in huSCs cultured at the given relative densities. (n = 150 cells per condition from three biological replicates) Error bars represent standard deviation. AU, arbitrary units.

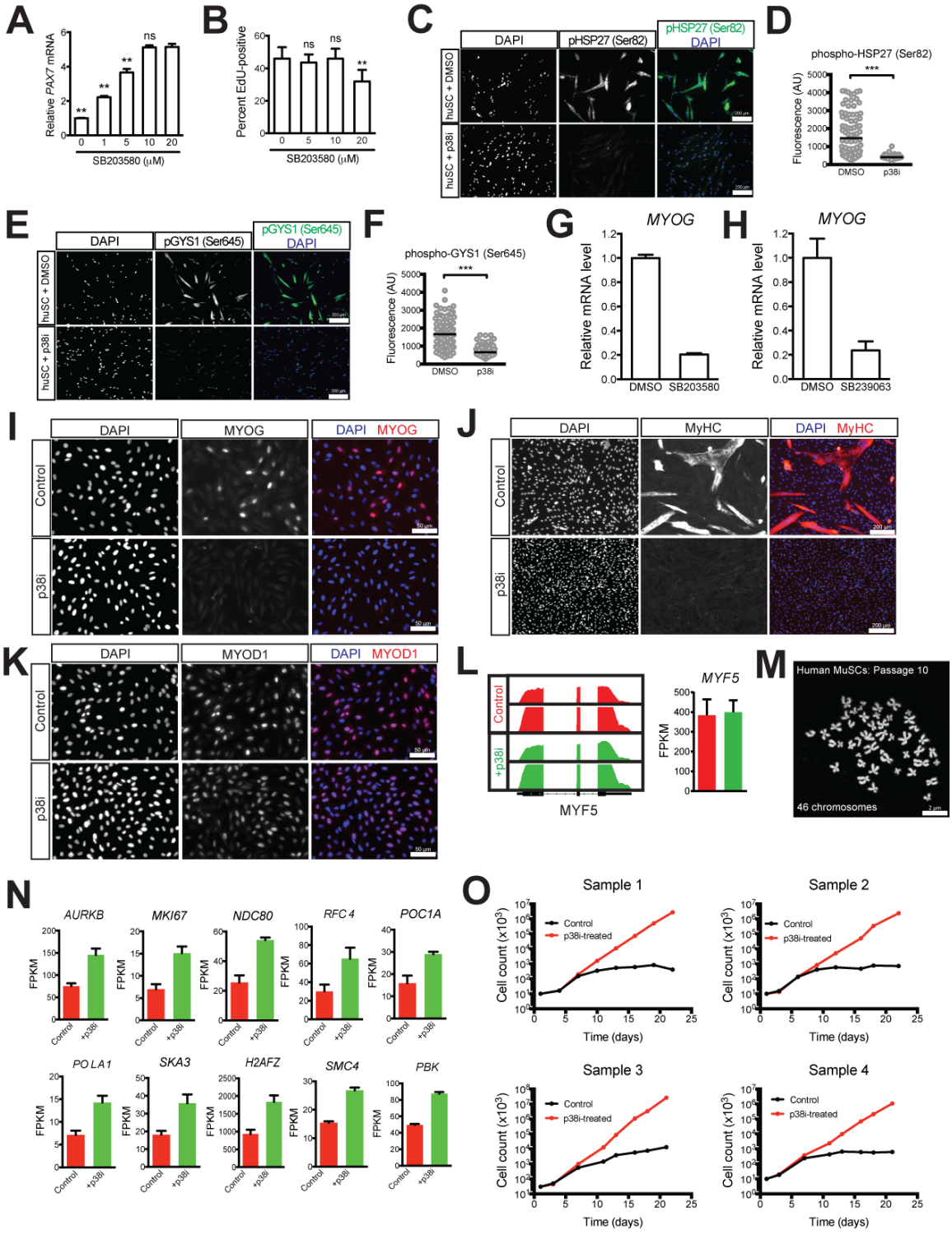
A
Relative PAX7 mRNA
SB203580 (μM)
B
Percent EdU-positive
SB203580 (μM)
C
DAPI
pHSP27 (Ser82)
pHSP27 (Ser82) DAPI
huSC + DMSO
huSC + p38i
D
phospho-HSP27 (Ser82)
Fluorescence (AU)
DMSO
p38i
E
DAPI
pGYS1 (Ser645)
pGYS1 (Ser645) DAPI
F
phospho-GYS1 (Ser645)
G
MYOG
Relative mRNA level
DMSO SB203580
H
MYOG
DMSO SB239063
I
DAPI
MYOG
DAPI MYOG
Control
p38i
J
DAPI
MyHC
DAPI MyHC
K
DAPI
MYOD1
DAPI MYOD1
L
Control
+p38i
MYF5
MYF5
FPKM
M
Human MuSCs: Passage 10
46 chromosomes
N
AURKB
MKI67
NDC80
RFC4
POC1A
POLA1
SKA3
H2AFZ
SMC4
PBK
FPKM
Control
+p38i
O
Sample 1
Sample 2
Sample 3
Sample 4
Control
p38i-treated
Cell count (x10^3)
Time (days)

Figure S3. Characterization of p38i effects on cultured SCs. Related to Figure 3. (A) Relative *PAX7* mRNA levels at given doses of p38i (SB203580) determined by RT-qPCR. Freshly isolated huSCs were cultured for 5 days prior to analysis. (n = 3) **(B)** Relative frequency of EdU incorporation after a one-hour EdU pulse at given doses of p38i. Cells were cultured for 3 days prior to analysis in order to analyze the effects on a more undifferentiated population of control cells. (n = 300 cells per condition from three biological replicates) **(C)** Representative IF analysis of phospho-HSP27 (Ser82) in SCs cultured for 8 days in the presence or absence of p38i. **(D)** Quantification of relative cytoplasmic fluorescence in IF analyses of phospho-HSP27 (Ser82) represented in (C). Each data point represents a single cell. **(E)** Representative IF analysis of phospho-GYS1 (Ser645) in SCs cultured for 8 days in the presence or absence of p38i. **(F)** Quantification of relative cytoplasmic fluorescence in IF analyses of phospho-GYS1 (Ser645) represented in (E). Each data point represents a single cell. **(G)** qRT-PCR analysis of relative mRNA expression of *MYOG* in huSCs cultured in the presence or absence of p38i (SB203580) for 6 days. (n = 3) **(H)** qRT-PCR analysis of relative mRNA expression of *MYOG* in huSCs cultured in the presence or absence of SB239063, an alternative p38 inhibitor, for 6 days. (n = 3) **(I)** Representative IF analysis of MYOG expression in control and p38i-treated huSCs. Cells were cultured for 6 days prior to analysis. While MYOG is observed in control cells, MYOG is absent from p38i-treated cells. **(J)** Representative IF analysis of MyHC expression in control and p38i-treated huSCs. Cells were cultured for 8 days prior to analysis. While MyHC is observed in control cells, MyHC is absent from p38i-treated cells. **(K)** Representative IF analysis of MYOD1 expression in control and p38i-treated huSCs. Cells were cultured for 6 days prior to

analysis. **(L)** RNA-sequencing analysis of *MYF5* expression in control (red) and p38i-treated (green) huSCs. Sequencing reads were mapped to the reference genome (left) and relative expression was quantified as FPKM (right). Error bars represent standard deviation; sequencing data are from two biological replicates per condition. **(M)** Representative micrograph of a metaphase chromosome spread of a human huSC cultured for 10 passages. **(N)** Expression of genes associated with DNA replication and cell division is increased in p38i-treated human huSCs relative to controls. Quantification of expression (FPKM) of representative genes in control (red) and p38i-treated (green) human huSCs. For all targets, expression levels differed significantly ($P < 0.05$) between control and p38i-treated samples. Error bars represent standard deviation. Sequencing data are derived from two biological replicates per condition. **(O)** Growth curves of huSCs isolated from four unique clinical specimens. Cultures derived from the same specimen were either left untreated (black) or maintained in the presence of p38i (red). Data for untreated samples are the same as those presented in Figure S1I. Cells were serially passaged to maintain a density of <40% confluence and were counted at each passage. $^{**}P < 0.01$, $^{***}P < 0.001$. AU, arbitrary units. ns, not significant ($P > 0.05$).

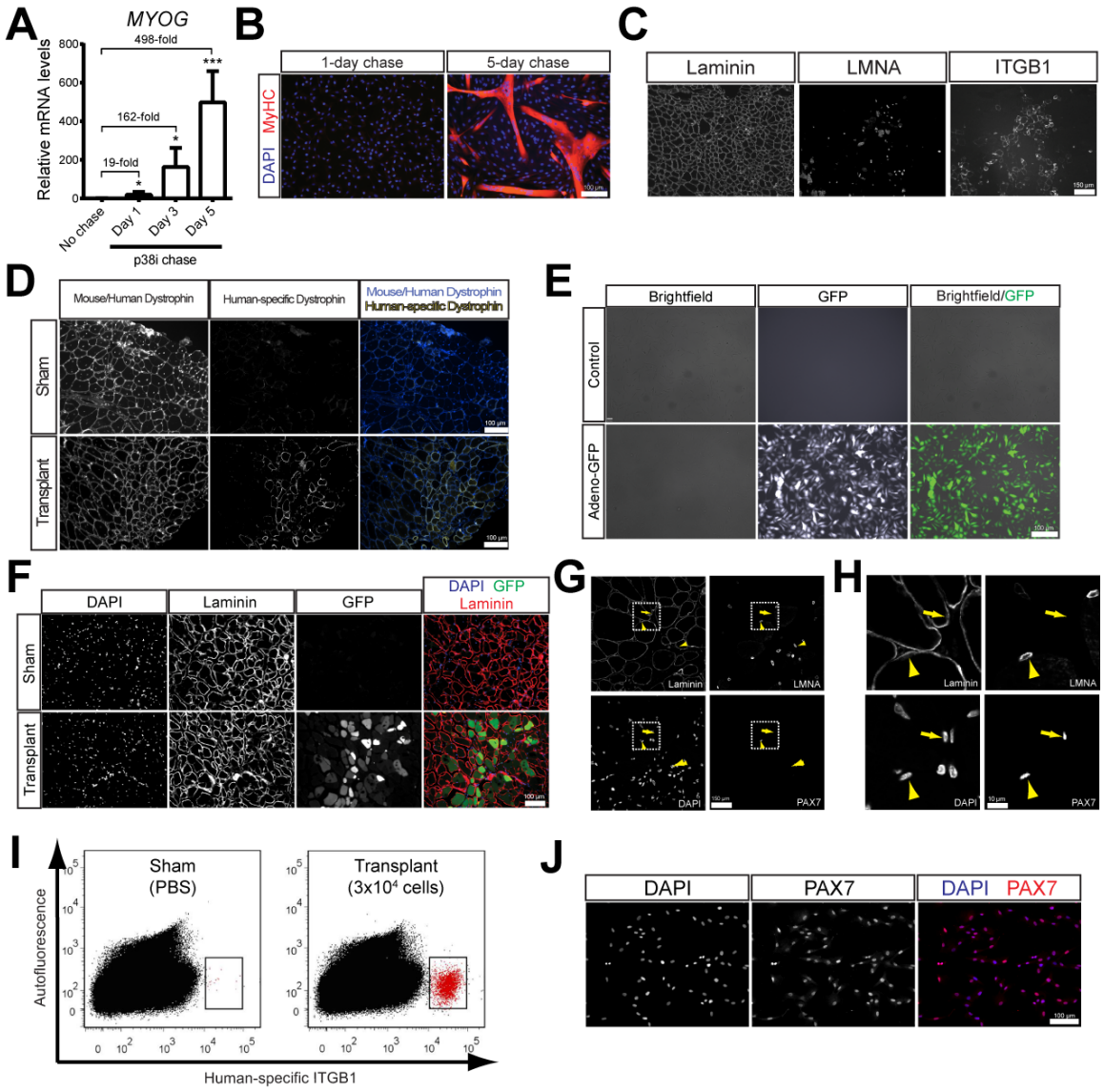
A
MYOG
Relative mRNA levels
800
600
400
200
0
498-fold
162-fold
19-fold
***
*
*
No chase
Day 1
Day 3
Day 5
p38i chase
B
1-day chase
5-day chase
DAPI MyHC
C
Laminin
LMNA
ITGB1
D
Mouse/Human Dystrophin
Human-specific Dystrophin
Mouse/Human Dystrophin
Human-specific Dystrophin
Sham
Transplant
E
Brightfield
GFP
Brightfield/GFP
Control
Adeno-GFP
F
DAPI
Laminin
GFP
DAPI GFP
Laminin
Sham
Transplant
G
Laminin
LMNA
DAPI
PAX7
H
Laminin
LMNA
DAPI
PAX7
I
Sham
(PBS)
Transplant
(3x10⁴ cells)
Autofluorescence
Human-specific ITGB1
J
DAPI
PAX7
DAPI PAX7

Figure S4. Differentiation and transplantation of expanded human huSCs. Related to Figure 4. (A) RT-qPCR analysis of *MYOG* mRNA levels over a period in which p38i was chased from the culture medium. huSCs were grown in p38i for 2 weeks, at which point p38i was removed, and cells were analyzed for mRNA levels at 1, 3 and 5 days after the chase began ($n = 3$). *$P < 0.05$, ***$P < 0.001$. Error bars represent standard deviation. **(B)** Representative IF images of MyHC expression in huSC cultures one (left) and five (right) days after p38i was removed from the culture. **(C)** Representative single-color images of human-specific ITGB1 expression in huSC-transplanted *tibialis anterior* muscles as presented in merged images in Figure 4A. Muscles were transplanted with 3×10^4 p38i-expanded huSCs and analyzed 28 days later. **(D)** Representative IF analysis of human/mouse-dystrophin and human-specific dystrophin expression in sham-treated and huSC-transplanted *tibialis anterior* muscles. Muscles were injected with PBS (sham) or transplanted with 3×10^4 p38i-expanded human huSCs and analyzed 56 days later. (**E**) Representative live-cell fluorescence micrograph of control (empty vector) and GFP-expressing adenovirus infected human huSCs. (**F**) Representative fluorescence microscopic analysis of muscle injected with PBS (sham) or transplanted with 3×10^4 GFP-expressing huSCs. Frozen sections of muscle were stained for human/mouse laminin to visualize muscle fiber boundaries. (**G**) Low- and (**H**) high-magnification images with individual colors that comprise the merged image in Figure 4B. The yellow arrowhead identifies a sublaminar PAX7-expressing cell of human origin; the yellow arrow identifies a nearby sublaminar Pax7-expressing cell of mouse origin. (**I**) Representative flow cytometric analysis of sham (PBS only) and transplanted (3×10^4

cells) muscles four weeks post-transplant. (**J**) IF analysis of PAX7 expression in the population of engrafted human huSCs re-isolated in (A). Nuclei were stained with DAPI.

Movie S1. Representative time-lapse videomicroscopy of *ex vivo* activation of purified human MuSCs. Related to Figure 1. The movie begins 12 h (t=0) post-isolation and continues for 90 h (t=90). Relative time is indicated in yellow.

Table S1. Transcription factors, receptors, and signaling molecules up-regulated in quiescent and activated huSCs. Related to Figure 2. Lists of the 30 most highly up-regulated transcription factors, receptors, and signaling molecules, as defined by the PANTHER gene ontology database, derived from RNA-seq comparisons of quiescent and activated huSCs. Loci for which the average FPKM was less than 5 were excluded.

Table S2. Biological processes associated with genes up-regulated in activated huSCs relative to quiescent huSCs. Related to Figure 2. Lists of biological processes, as defined by the PANTHER gene ontology database, significantly enriched ($P < 0.05$) among genes up-regulated in activated relative to quiescent huSCs. Gene set enrichment was analyzed using the DAVID bioinformatics platform. The associated genes are listed with each term. The analysis used those loci for which FPKM>5 and fold-change >2.

Table S3. Biological processes associated with genes up-regulated in quiescent huSCs relative to activated huSCs. Related to Figure 2. Lists of biological processes, as defined by the PANTHER gene ontology database, significantly enriched ($P < 0.05$)

among genes up-regulated in quiescent relative to activated huSCs. Gene set enrichment was analyzed using the DAVID bioinformatics platform. The associated genes are listed with each term. The analysis used those loci for which FPKM>5 and fold-change >2.

Table S4. Biological processes associated with genes differentially expressed by human p38i-treated huSCs relative to untreated huSCs. Related to Figure 3. Lists of biological processes, as defined by the PANTHER gene ontology database, significantly enriched ($P < 0.05$) among genes with increased or decreased expression in p38i-treated huSCs relative to untreated huSCs. Gene set enrichment was analyzed using the DAVID bioinformatics platform. The associated genes are listed with each term. The analysis used those loci for which FPKM>5 and fold-change >2.

SUPPLEMENTAL EXPERIMENTAL PROCEDURES

Human skeletal muscle specimens

Reproducibility of prospective isolation methods was also tested with *serratus anterior* and *rectus abdominis* muscle specimens. Subjects ranged in age from 35 to 82 years. Scarcity of samples did not allow for statistically meaningful comparisons of samples according to donor age. Sample processing for cell or tissue analysis began within one hour of specimen isolation. In all studies, standard deviation reflects variability in data derived from studies using true biological replicates (i.e., unique donors). Data were not correlated with donor identity.

Human SC isolation

After triturating and washing the digested muscle to yield a mononuclear cell suspension, the cells were stained for 45 min at 4°C with anti-CD31-Alexa Fluor 488 (clone WM59; BioLegend; #303110), anti-CD45-Alexa Fluor 488 (clone HI30; Invitrogen; #MHCD4520), anti-CD34-FITC (clone 581; BioLegend; #343503), anti-ITGB1-APC (clone TS2/16; BioLegend; #303008) at 1:100 (V:V). In addition to primary antibodies, cells were incubated with EGF-biotin (Invitrogen; #E3477) at 0.4 μg/mL to detect EGFR. After washing away primary antibodies, cells were incubated for 15 min at 4°C in streptavidin-PE/Cy7 (BioLegend) at 1:100 (V:V) to detect EGF-biotin. Cell sorting was performed with a BD FACSAria II or BD FACSAria III using 405-nm, 488-nm, and 633-nm lasers. Sorted cells were routinely analyzed by flow cytometry immediately after sorting to ensure high sorting efficiency. Unstained cells were routinely

used to define FACS gating parameters. A fraction of the sorted cells were routinely plated and stained for PAX7 to determine the purity of the sorted population.

Human muscle fiber explants and immunofluorescence analysis

Isolated fibers were washed in media and fixed in 4% PFA (PBS). Fibers were permeabilized with 0.3% Triton X-100, blocked in 10% goat serum, and stained overnight with primary antibodies against surface markers (same as those used for sorting) and against PAX7 (DSHB) at 1:100 (V:V). After washing out primary antibodies, fibers were stained with secondary antibodies and DAPI. Anti-mouse antibodies raised in goat and conjugated to Alexa Fluor 594 (Invitrogen) or Alexa Fluor 488 (Invitrogen) were used to detect PAX7. For EGFR analysis, unfixed fibers were incubated for 15 min in EGF-biotin, fixed in 4% PFA (PBS), and stained as above. Streptavidin-Alexa Fluor 647 was used to detect the EGF-biotin. After washing out secondary antibodies, muscle fiber explants were mounted on microscope slides (Superfrost Plus; Fisher Scientific).

Human SC culture

Differences in the expression of *PAX7*, *PAX3*, *MYF5* and *MYOG* among SCs cultured in media containing different serum lots were not statistically significant (data not shown). Where indicated, medium was supplemented with 10 μM p38 inhibitor (SB203580, Cell Signaling Technology; SB239063, Tocris Bioscience). Medium, including medium containing p38i, was changed once every two days. Where indicated, EdU (Invitrogen) was pulsed for 1 h at a final concentration of 10 μM. Cells were

routinely cultured at densities of 40% confluency, except where indicated. To test for myotube formation, huSCs or huSC-depleted cells were cultured for 9 days with a target final confluency of ~90%.

For clonal analyses, purified cells were plated singly in ECM-coated chamber slides, and cultured as above for a period of six days. In the putative SC population, a total of 140 clones were analyzed. In the non-myogenic population of CD31, CD45, or CD34-expressing cells, 125 clones were analyzed. These clones were cultured in two independent experiments. For comparisons of p38i effects on EdU incorporation in undifferentiated cultures, freshly isolated cells were grown in the given concentration of p38i for a period of 3 days. EdU (10 μM) was added to the culture for 1 h prior to fixation. For comparisons of p38i effects on EdU incorporation in differentiated cultures, cells were grown in the given concentration of p38i for a period of 9 days. For analyses of p38 target gene expression, cells were cultured for 9 days with a target final confluency of 80%.

For analysis of engraftment of GFP-expressing, p38i-expanded huSCs, cells were initially expanded for 10 d and then infected with adenovirus bearing a GFP reporter gene (Ad5CMV-GFP; University of Iowa Gene Transfer Vector Core) or vector control (Ad5CMV-empty). Medium was replaced 24 h post-transfection, and cells were further expanded for >3 additional passages prior to transplantation. Infection efficiency was routinely monitored by epifluorescence microscopy (see Figure S4E).

Quantitative RT-PCR

One microgram of total RNA was reverse-transcribed using the High Capacity cDNA Reverse Transcription Kit (Invitrogen). Quantitative PCR was performed on an ABI 7900HT Fast Real-Time PCR system using custom synthesized oligonucleotide primers (Invitrogen) designed to amplify the cDNA of selected target genes. Relative quantification of gene expression normalized to GAPDH was carried-out using the comparative C_T method (Pfaffl, 2001). Each measurement was performed in triplicate in two independent experiments. The following primers were used in these assays:

Target	Forward Primer	Reverse Primer
PAX7	gaaaacccaggcatgttcag	gcggctaatcgaactcactaa
PAX3	ttggcaatggcctctcac	aggggagagcgcgtaatc
MYF5	ctatagcctgccgggaca	tggaccagacaggactgttacat
MYOD1	cactacagcggcgactcc	taggcgccttcgtagcag
MYOG	gctcagctccctcaacca	gctgtgagagctgcattcg
MEF2C	tgatcagcaggcaaagattg	tggacactgggatggagact
GAPDH	agccacatcgctcagacac	gcccaatacgaccaaatcc

Immunofluorescence analysis of cultured SCs

Cultured SCs were fixed with ice-cold 4% PFA (in PBS) for 10 min, rinsed with PBS, and permeabilized in 0.3% Triton X-100 (in PBS). Fixed and permeabilized cells were blocked in 10% goat serum (in PBS) and incubated with primary antibodies for 12 h at 4°C. Primary antibodies recognizing PAX7 (DSHB), MYOD1 (clone 5.8A, Dako, #M3512), MYOG (clone F5D, DSHB), and myosin heavy chain (clone MF20, DSHB) were used at 2.5 μg/mL, 2.8 μg/mL, 1.6 μg/mL, and 0.5 μg/mL, respectively. Primary

antibodies recognizing p-p38 (Cell Signaling, #9211), phospho-HSP27 (Ser82) (Cell Signaling, #9709), and phospho-GYS1 (Ser645) (Abcam, ab195743) were each used at 1:200 (V:V). After washing-out primary antibodies with PBS, cells were incubated with secondary antibodies for 1 h at room temperature. Anti-mouse antibodies raised in goat and conjugated to Alexa Fluor 594 or Alexa Fluor 488 were used to detect mouse primary antibodies. EdU detection was carried-out using a Click-It EdU detection kit (Life Technologies) according to the manufacturer's instructions. Cells were next washed with PBS and mounted with Fluoro-Gel (Electron Microscopy Sciences). IF imaging was performed with an AxioObserver Z1 epifluorescence microscope (Carl Zeiss) equipped with an Orca-R2 CCD camera (Hamamatsu Photonics) or an LSM 710 confocal system (Carl Zeiss). Image analysis was performed using Improvision Volocity software (Perkin Elmer) or ZEN 2010 software (Carl Zeiss). For quantitation of purity in cultured purified SCs, the proportion of cells expressing PAX7 was calculated 3 days after cell isolation in 8 representative cultures each derived from a distinct donor. For quantification of relative fluorescence intensity, Improvision Volocity software was used to define a ROI for each cell, and the average fluorescence intensity in the channel of interest for a given cell was calculated by the software. Fluorescence intensity measurements for single cells was recorded. In the case of p-p38 fluorescence measurements, the nucleus (defined by area stained with DAPI) was used for the ROI; in the case of p-GYS1 and p-HSP27, the entire cell (defined by phase-contrast) was used for the ROI.

Metaphase spreads

Human SCs were cultured as described above. Colcemid was added to the culture at a final concentration of 100 ng/mL for 3 h. Culture medium was collected and the cells were incubated for 15 min in Trypsin-EDTA at 37^{o}C. Trypsinized cells were combined with the collected medium, centrifuged, and gently resuspended in 0.3 mL of medium. Seven mL of hypotonic solution (0.8% sodium citrate in water) was added dropwise to the sample and incubated for 10 minutes at room temperature. The sample was then washed and resuspended in 0.5 mL of hypotonic solution. Seven mL of Carnoy's fixative (3:1 methanol:acetic acid) was added and incubated for 10 minutes at room temperature. Fixed cells were then washed an additional two times in fixative. Cells were resuspended in 500 mL of fixative and dropped onto SuperFrost Plus microscope slides from a height of 1.5 m. Once dry, slides were mounted with DAPI-containing Fluoro-Gel. Spreads were imaged with a Zeiss LSM 710 confocal system. A total of 75 metaphase cells from three independent experiments were analyzed.

Time-lapse microscopy

Prospectively isolated human SCs were plated at a density of 2,500 cells per 0.7 cm^2 and cultured as above. Cultures were analyzed using an Axiovert 200M inverted microscope (Carl Zeiss) equipped with an environmental control chamber (CTI controller, Tempcontrol; Carl Zeiss; humidified 5% CO_2). Brightfield images were obtained every 15 min for 4 days with a Zeiss camera controlled with the Axiovision software (Carl Zeiss). All calculations of cell-cycle times were performed on a total of 200 cells from three independent experiments.

RNA isolation, sequencing and analysis

Total RNA was extracted from FACS-purified SCs using the NucleoSpin RNA XS (Macherey-Nagel #740902). Two biological replicates were sequenced in each of three conditions (freshly isolated, cultured, and cultured in the presence of p38i). All muscle tissue used in these analyses was from *latissimus dorsi*. Cultured cells were maintained at <40% confluency prior to RNA isolation. For Illumina sequencing, cDNA libraries were generated with 500 pg of total RNA using the SMARTer Ultra Low Input RNA Kit for Illumina Sequencing (Clontech #634935). Paired-end sequencing libraries were then generated using the Ovation Ultralow Library System (NuGEN #0303) according to manufacturer instructions. The libraries were sequenced on an Illumina HiSeq 2000 at the Stanford Center for Genomics and Personalized Medicine. Approximately 200 millions paired-end reads (2x100bp) were obtained per biological replicate. Paired-end reads were filtered, aligned to the hg19 genome assembly and quantified as the number of sequenced fragments per kilobase of exon per million fragments mapped (FPKM) using the Tuxedo protocol (Trapnell et al., 2012).

Gene set enrichment and transcription factor network analysis

Gene set enrichment analysis was performed with the DAVID Functional Annotation tool (Huang et al., 2009). Gene sets were defined as noted in the text, typically using thresholds of 5- to 10-fold change in FPKM between samples.

To build a transcription factor network reflecting the regulation of huSC activation from a quiescent state, we first used the Whole Genome rVista tool to identify transcription factors with predicted binding sites that are over-represented ($P < 3x10^{-7}$) in

upstream regions (within 3000 bp) of the genes for which expression differs more than ten-fold between quiescent and cultured huSCs after a period of 7 days in culture. FPKM values from RNA-seq analyses were used to calculate gene expression changes. Using the identified transcription factors as nodes, we constructed a network based on known interactions among transcription factors using STRING version 9.05 (Franceschini et al., 2013). Disconnected or singly connected nodes were excluded from the network.

Animals

NOD/SCID and IL2 receptor gamma chain deficient (NSG) mice were obtained from The Jackson Laboratory. Mice were housed and maintained in the Veterinary Medical Unit at Veterans Affairs Palo Alto Health Care Systems. Male mice aged 2 to 4 months were used in our studies. Animal protocols were approved by the Administrative Panel on Laboratory Animal Care of the VA Palo Alto Health Care System.

Human SC transplantation

NSG mice were used as transplant recipients. The *tibialis anterior* muscle of the recipient mouse was injured with 50 μL of 1.2% $BaCl_2$ 48 h prior to use in transplantation studies. Cultured human SCs were incubated in Accutase (Invitrogen) at 37°C to detach cells, resuspended in fresh DMEM, and filtered through a 40-μM cell strainer to exclude any fused myotubes. Freshly isolated and cultured SCs were counted, centrifuged, and resuspended in a volume of 1% BSA (in PBS) that would enable transplantation of the appropriate dose of cells in a total volume of 15 μL per transplantation. Cell suspensions were kept on ice prior to transplantation. For

transplantation, cells were loaded into a 50-μL Hamilton syringe equipped with a 30-gauge needle. After incising the skin overlying the anterior lower hindlimb, 3×10^4 cells were delivered to the *tibialis anterior* muscle as a single injection. Recipient mice were treated post-surgery with buprenorphine (0.1 mg/kg) and baytril (5 mg/kg). All quantitative analyses of transplantation were performed on a minimum of four biological replicates per tested condition.

Histological analysis of SC engraftment

Four to eight weeks post-transplantation, recipient *tibialis anterior* muscles were dissected and frozen by immersion for 90 s in liquid nitrogen-cooled isopentane. For analysis of GFP expression, muscles were fixed for 6 h in 0.5% PFA (in PBS) and dehydrated in 20% sucrose (in PBS) for 12 h before freezing. Frozen muscles were stored at -80°C prior to sectioning. Cross-sections of transplanted muscle were cut at a thickness of 7 μm, collected onto Superfrost Plus glass slides, rehydrated with PBS, and fixed in 4% PFA (in PBS) for 5 min. After washing with PBS, sections were permeabilized with 0.3% Triton X-100 for 10 min and again washed with PBS. Sections were then blocked for 1 h in 10% goat serum (in PBS) or, when unconjugated mouse primary antibodies were used, in 10% goat serum (in PBS) with mouse-on-mouse blocking reagent (Vector Laboratories) according to the manufacturer's instructions. Blocking solution was washed away with PBS and sections were incubated overnight with primary antibodies at 4°C. Sections were then washed with PBS and incubated with secondary antibodies, and DAPI, for one hour at room temperature. Secondary antibodies were washed away with

PBS and slides were mounted with Fluoro-Gel. Imaging was performed as described above.

Primary antibodies used for staining frozen sections were: mouse anti-PAX7 (detecting human and mouse; DSHB; 2.5 μg/mL), mouse anti-DMD (human-specific; EMD Millipore #MAB1690; 1:20 V:V), rabbit anti-DMD (detecting human and mouse; Abcam #15277; 1:500 V:V), rabbit anti-LMNA (human-specific; clone EPR4100; Abcam #108595; 1:300 V:V), rat anti-laminin (detecting human and mouse; clone 4H8-2; Abcam #11576; 1:2500 V:V), and mouse anti-ITGB1 (human-specific; clone TS2/16; BioLegend; #303008; 1:200 V:V) conjugated to APC. Primary antibodies were detected with secondary antibodies recognizing mouse, rat or rabbit conjugated to Alexa Fluor dyes.

SUPPLEMENTAL REFERENCES

Franceschini, A., Szklarczyk, D., Frankild, S., Kuhn, M., Simonovic, M., Roth, A., Lin, J., Minguez, P., Bork, P., von Mering, C., et al. (2013). STRING v9.1: protein-protein

interaction networks, with increased coverage and integration. Nucleic Acids Res. *41*, D808–D815.

Huang, D.W., Sherman, B.T., and Lempicki, R.A. (2009). Systematic and integrative analysis of large gene lists using DAVID bioinformatics resources. Nat. Protoc. *4*, 44–57.

Pfaffl, M.W. (2001). A new mathematical model for relative quantification in real-time RT-PCR. Nucleic Acids Res. *29*, e45.

Trapnell, C., Roberts, A., Goff, L., Pertea, G., Kim, D., Kelley, D.R., Pimentel, H., Salzberg, S.L., Rinn, J.L., and Pachter, L. (2012). Differential gene and transcript expression analysis of RNA-seq experiments with TopHat and Cufflinks. Nat. Protoc. *7*, 562–578.